https://doi.org/10.5194/egusphere-2026-4202
Preprint. Discussion started: 14 August 2026

Coarsening of fluvial sediments after the Gorkha Earthquake 2015, Nepal

David Puhl[1,2], Jens M. Turowski[2], Christoff Andermann[3,2], Michael Dietze[4,2], Kristen L. Cook[5], Gen K. Li[6], Basanta R. Adhikari[7]

[1]Department of Geography, University of British Columbia, Vancouver, BC, Canada
[2]Section 4.6 Geomorphology, German Research Centre for Geosciences GFZ, Helmholtz Zentrum Potsdam, Telegrafenberg, 14473 Potsdam, Germany
[3]Univ Rennes, CNRS, Géosciences Rennes, UMR 6118, 35000 Rennes, France
[4]Department of Geography, RWTH Aachen University, Wüllnerstraße 5b, D-52062 Aachen, Germany
[5]ISTerre, Université Grenoble Alpes, IRD, Grenoble, France
[6]Department of Earth Science, University of California, Santa Barbara, CA 93106, USA
[7]Department of Civil Engineering, Pulchowk Campus, Institute of Engineering, Tribhuvan University, Nepal

Correspondence to: David Puhl (davidp@student.ubc.ca)

Abstract. In April, 2015 the M_w 7.8 Gorkha Earthquake hit central Nepal, causing widespread co- and post-seismic landsliding. Such surface processes have the potential to increase erosion and perturb fluvial systems for years to decades. Although mass wasting is known to supply coarse material to channels, its impact on the grain size characteristics of suspended sediments remains poorly understood. Here, we present time-series grain size distribution data collected during 2015-2018 from four hydrologic stations using a nested catchment approach in the Koshi basin, where abundant landslides occurred after the Gorkha event. We analyse post-earthquake grain size distribution of riverine suspended sediment and landslide deposit using an end-member modelling analysis. Our results exhibit statistically distinctive signals. We find that one of the coarsest grain size end members (~400 mm) is particularly dominant in the two smallest catchments in the monsoon immediately following the earthquake in 2015. This grain size end member is also abundant in our co-seismic landslide deposit samples, indicating that the higher presence of this end member at our upstream stations likely relates to sediment supply from co- or post-seismic landslides. The earthquake signal in the suspended sediment is only present during the 2015 monsoon season, suggesting that the fine sediment transport in central Nepal was only perturbated by the earthquake for about one season. This provides novel and valuable process-based insight that elevated landslide activity leads to coarsening of suspended load in small catchments. However, it seems unlikely that this signal is recorded in far downstream depositional basins as it is lost during transport.

https://doi.org/10.5194/egusphere-2026-4202
Preprint. Discussion started: 14 August 2026

1 Introduction

The grain size of fluvial sediments is largely influenced by the type and magnitude of sediment supply (Attal et al., 2015; Sklar et al., 2020; Chen et al., 2025; Li et al., 2025; Yanites et al., 2025). Topographic, lithological, climatic, and land cover factors constrain the grain size of sediment supplied to channels and therefore the grain size of fluvial sediments. Consequently, the grain size distribution of fluvial sediments reveals insights into sediment sources and transport processes (Riebe et al. 2015, Struck et al. 2015, Attal et al. 2015, Abbott et al. 2018, East et al. 2018, Sklar et al. 2020). Moreover, the type of sediment supply process determines the grain size distribution of sediment export (e.g., Roda-Boluda et al. 2018, Tofelde et al. 2018) and therefore of the stratigraphic records and the architecture of sedimentary basins (e.g., Armitage et al. 2011, Allen et al. 2015, Romans et al. 2016). If grain size information is preserved in sedimentary archives over geological time spans, sediment supply processes to the archive can be reconstructed, possibly documenting the environmental conditions during erosion, transport and deposition of these sediments (e.g., Romans et al. 2016, Tofelde et al. 2021, Zeichner et al. 2021). Although, grain size signatures of supplied sediments will be modified in the channel due to in-stream processes like selective entrainment and abrasion of bedload particles and bedrock largely depending on underlying lithology (e.g., Dingle et al. 2017, Attal and Lave 2009, Pokhrel et al., 2024).

Suspended sediments are generally thought to be mainly supply-limited, especially in high energy environments like steep Himalayan rivers, where fluvial transport capacity is high and capable of evacuating all supplied sediments (e.g. Vanoni, 1975; Andermann et al. 2012). Grain size characteristics of suspended sediments therefore might largely depend on supply rather than hydrologic processes and are able to be routed through the system without significant size selective modifications (Andermann et al., 2012; Morin et al., 2018). Hence, signals of input processes might be traced reliably downstream to the zone of dilution, where the signal declines below the detection limit. In mountain environments with steep slopes most sediment entering the river is supplied by hillslope processes. Landsliding is a significant agent in the physical erosion of mountain ranges (e.g., Hovius et al. 1997, Li et al. 2019). Mobilization of material by landslides affects sediment discharge in rivers on various scales depending on the type and rate of landsliding (Pearce & Watson 1986, Hovius et al. 2000, Martin et al. 2002, Koi et al. 2008, Benda & Dunne 1997).

Strong earthquakes in mountainous areas are accompanied by widespread co-seismic mass wasting (Keefer, 1984 & 1994, Roback et al. 2018, Meunier et al. 2007 & 2008). Hillslope stability can be affected for far longer than the time span of the main shock or associated aftershocks, with elevated landslide activity for up to several years following the earthquake (Marc et al. 2015, Parker et al. 2015, Yang et al. 2017, Burrows et al, 2023, Illien et al., 2025). This is generally termed post-seismic mass wasting. Increase in landsliding due to large earthquakes are thought to translate into changes in sediment transport and export in the river network, leading to elevated sediment concentration for a few years (Hovius et al. 2011). However, this phenomenon has been observed only for two major events so far: the 1999 Chi Chi Earthquake (Dadson et al. 2004, Lin et al. 2008, Yanites et al. 2010) and the 2008 Wenchuan Earthquake (Parker et al. 2011, Wang et al. 2015, Li et al. 2016). Evidence from the Wenchuan Earthquake in 2008 suggests that bedload fluxes remained far above pre-earthquake levels for a decade (Li et al., 2025), highlighting how such disturbances can amplify sediment supply for extended periods. Moreover, earthquake-conditioned landscapes may be especially vulnerable to subsequent flood-driven sediment export (Chen et al., 2025). More broadly, large-scale perturbations such as earthquakes are known to amplify cascading geomorphic responses, including accelerated erosion and deposition that can persist from months to decades due to the larger volumes of sediment stored in channels (Yanites et al., 2025). Thus, the amplitude and duration of earthquakes on river sediment loads, and their expression in the sediment granulometry, require further attention, as well as their relation to the dynamics of the upstream and upslope sediment sources.

Using grain size information as signal for environmental conditions in the past has a long tradition in Earth science applications (Folk and Ward 1957, Flemming 2007). Grain size distributions, the fraction in a certain grain size range, ratios of grain size fraction, or cumulative percentiles have been used as paleoclimate proxies (e.g. Vandenberghe et al., 1985, 1997, Beget 1990). Recently, it has been demonstrated that different grain sizes can carry different information (Lukens et al, 2023). However, sampled grain size distributions are typically mixtures of subpopulations due to different sorting, transport, and deposition processes. The individual proportion of each grain size population is usually unknown, and therefore the unequivocal interpretation of multimodal grain size data is challenging. Decomposition of grain size distributions into their original subpopulations can be achieved by a statistical approach called end-member modelling analysis - EMMA (Weltje and Prins, 2007, Dietze et al. 2012, 2014, Dietze and Dietze, 2019a). This technique allows one to describe a multimodal grain size data set by a finite number of underlying subpopulations. The technique then extracts the relative contributions of each end member within each sample and thereby overcoming the problem of mixed information.
In this study, we investigate the change in the grain size characteristics of suspended sediments from a major Himalayan river system following the Gorkha Earthquake, which affected wide parts of the Nepal Himalayas on April 25th in 2015. We assess the earthquake-specific grain size signature and explore how far downstream from directly affected areas an earthquake-induced grain size signal can propagate and over which time scale that signature diminishes.

2 Regional Context

The Himalayan mountain range is the product of the active continental convergence of the Indian and Eurasian Plates. The southern front is subject to a monsoon climate, with distinct annual wet and dry seasons controlled by the Indian Summer Monsoon (ISM), which usually occurs from June to September (Hannah et al., 2005). About 80 % of the mean annual precipitation, ranging in Nepal from 1,000 to 3,500 mm (Talchabhadel et al. 2018), falls during the ISM season and only a minor part during the non-ISM season (Andermann et al., 2011). The distribution of rainfall across the mountain range is strongly impacted by orographic effects, resulting in a three- to four-fold increase from the southern lowlands to elevations of about 4000 m. Rainfall drops to a minimum of about 250 mm/yr on the Tibetan plateau. Annual precipitation totals along the

Himalayan front of Nepal are typically less than 1500 mm/yr and can locally reach more than 4000 mm/yr (Andermann et al., 2011, Bookhagen and Burbank, 2006).

Due to steep mountainous terrain and the annual intense rainfall events during the ISM, the Himalayas experience high rates of erosion. Based on fluvial suspended sediment export measurements, short-term (1-10 years) average erosion rates range between 0.1 and 2.0 mm/yr for small (100-3000 km2) catchments (Gabet et al., 2008). Main catchments draining the Himalayan mountain belt show erosion rates derived from suspended sediment between 1-2 mm/yr (Andermann et al., 2012; Struck et al., 2015; Morin et al., 2018). These short-term erosion rates are comparable to 10Be derived erosion rates integrating over 100 to 1000 years (Lupker et al. 2012).

2.1 The 2015 M_w 7.8 Gorkha Earthquake

The Nepal Himalayas are one of the seismically most active mountain belts in the world and have a history of strong earthquakes. On 25 April 2015, the magnitude (Mw) 7.8 Gorkha Earthquake ruptured a ~140 km long, east-west segment of the Main Himalayan Thrust, but did not produce a surface rupture (Zhang et al. 2016, Kobayashi et al. 2015, Elliot et al. 2016). It was a thrust earthquake with an epicenter near Barpa in the Gorkha district, 80 km northwest of Kathmandu. The rupture propagated to the southeast leading to high ground motions to the east of the epicenter (Avouac et al. 2015, Zhang et al. 2016, Koketsu et al., 2016). The main shock was followed by 553 >Mw 4.0 aftershocks within the first 45 days after the main shock (Adhikari et al. 2015), including a magnitude Mw 7.3 aftershock on the 12th of May 2015, at the eastern end of the main rupture.

2.2 Co- and post-seismic landslides caused by the Gorkha Earthquake

The Gorkha Earthquake caused catastrophic damage in a wide area by landsliding, rock fall, and earth cracks. A number of studies focused on mapping of co-seismic landslides (Kargel et al. 2016, Xu et al. 2016, Martha et al. 2017, Tiwari et al. 2017, Williams et al. 2018, Roback et al. 2018, Gnyawali & Adhikari 2017, Valagussa et al. 2021), finding total numbers of co-seismic landslides ranging from around 5,000 to 25,000 over an affected an area larger than 30,000 km². Landslide activity was mainly concentrated in the metamorphic Lesser and Greater Himalayan rock. Most landslides were rockslides primarily in zones with weak weathered rock, which are concentrated on the steeper parts of the slopes along the ridges (Zekkos et al., 2017).

Rainfall-induced post-seismic landslide rates in three selected catchments were ~3-6 times higher in the 2015 ISM than in pre-earthquake ISM but had recovered to the pre-earthquake level by 2016 (Marc et al. 2019). Similar results have been reported for debris flows, which predominantly occurred in the monsoon 2015 and returned to pre-earthquake levels by 2016 (Dahlquist and West, 2019). However, Tian et al. (2020) observed the evolution of 30 co-seismic landslides and reported that most of

https://doi.org/10.5194/egusphere-2026-4202
Preprint. Discussion started: 14 August 2026

them stayed active for three years by enlarging or remobilization of material into debris flows. Rosser et al. (2021) and Kincey et al. (2021) observed elevated landslides rates for their study period of 4.5 years. In their compilation, Kincey et al. (2021) included active historical landslides, if bare earth was still visible, assuming that they were still susceptible to new failures or mobilization of landslide debris relevant for geohazard assessment. In contrast, Marc et al. (2019) counted only new landslide failures in any given observation time interval.

2.3 Study Area

The Koshi drainage basin is situated in east-central Nepal, within the Himalayan mountain range and parts of the Tibetan plateau. It is the eastern most of three major watersheds that drain most of Nepal and large parts of the Tibetan Plateau. We sampled suspended load along the Bhote-Sun-Sapta-Koshi river system and in the Kahule Khola, a small tributary of the Bhotekoshi (Fig. 1, Illien et al., 2021). The smallest catchment in our study, the Kahule Khola, drains 32 km^2 and joins the Bhotekoshi with a catchment area of 2,400 km^2, which joins the Sunkoshi draining 10,000 km^2, which finally joins the Saptakoshi draining 54,024 km^2 (Knight et al., 2024, see Table 1 for morphometric description of the catchments). Even before the Gorkha event, the Bhotekoshi catchment has been a landslide-prone area, where landslides triggered by intense rainfall are a common occurrence during the monsoon season (Andermann & Gloaguen, 2009).

Table 1: Morphometric description of study catchments.

	Kahule Khola	**Bhotekoshi**	**Sunkoshi**	**Saptakoshi**
Max elevation (m)	3459	7928	7928	8773
Min elevation (m)	1111	876	455	141
Mean elevation (m)	2293	4527	3210	2930
Relief (m)	2348	7052	7473	8632
Mean catchment slope (°)	32	26	27	27
Hypsometric intergral (HI)	0.50	0.52	0.37	0.32
Gravelius compactness coefficient (Sassolas-Serrayet et al., 2018)	1.8	2.3	2.0	2.6
Drainage density (km/km^2)	0.38	0.59	0.55	0.54
Number of landslides (Roback et al., 2018)	408	4,381	13,712	13,817

https://doi.org/10.5194/egusphere-2026-4202
Preprint. Discussion started: 14 August 2026

Landslide density (km²/km²)	0.0147	0.0058	0.0041	0.0016
Lithology*	10% Schist 43% Dolomite 47 % Granite and Gneiss	1% Shale 2% Quartzite 3% Phyllite 7% Dolomite 87% Granite and Gneiss	1% Marble 6% Dolomite 7% Quartzite 14% Schist 21% Phyllite 52% Granite and Gneiss	1% Shale 3% Dolomite 4% Quartzite 23% Phyllite 23% Schist 46% Granite and Gneiss

*Does not include coverage on the Tibetan Plateau

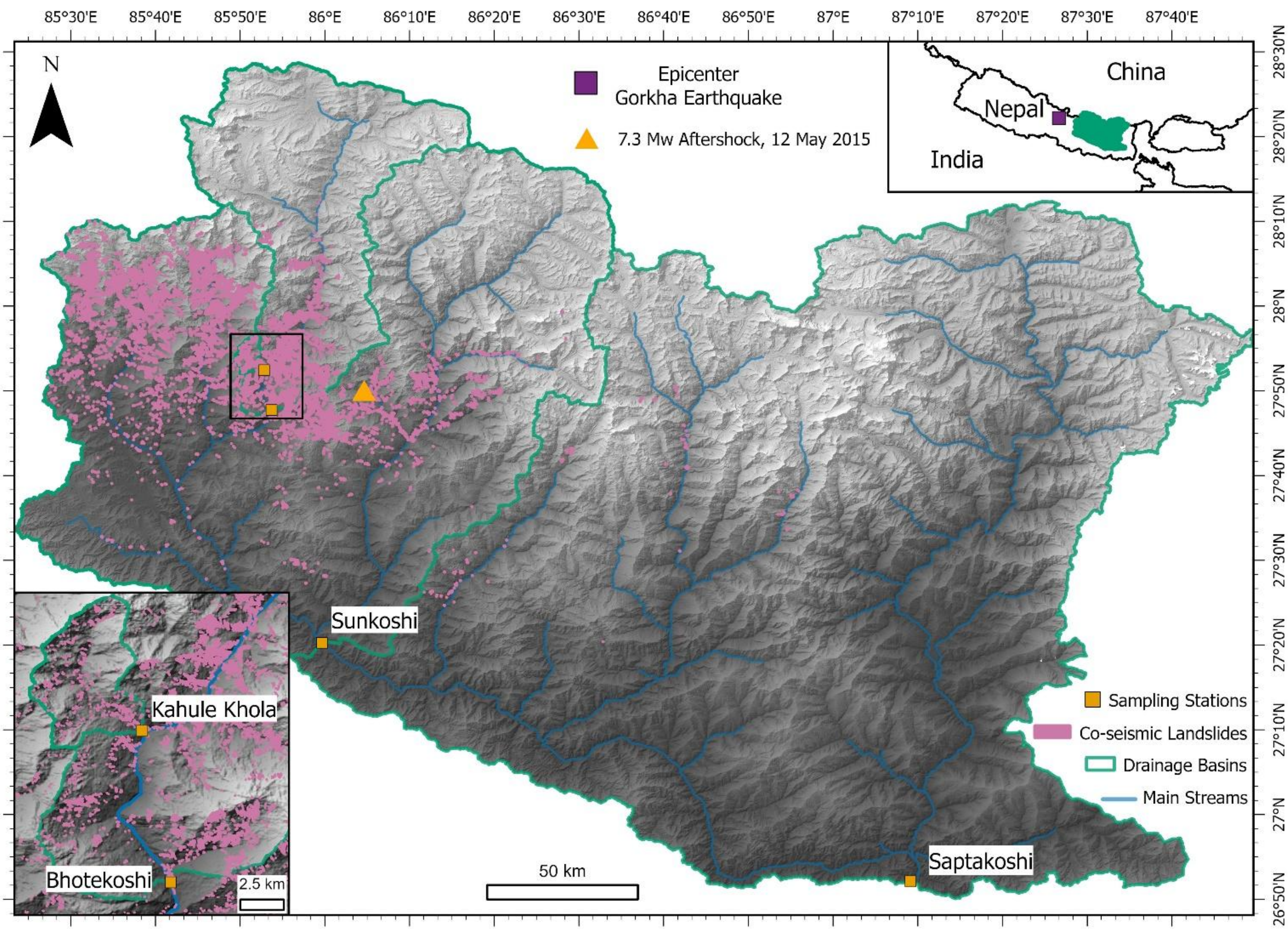

Figure 1: Overview of Koshi drainage basin and respective sampling stations within the nested catchment approach. Furthermore, the distribution of landslides trigger by the 2015 Gorkha Earthquake are shown in pink (see Roback et al. 2018).

https://doi.org/10.5194/egusphere-2026-4202
Preprint. Discussion started: 14 August 2026

During the Gorkha Earthquake, landslides concentrated in the western part of the Koshi drainage area and mainly affected the Bhotekoshi and Kahule Khola catchment (Fig. 1). Half of the rupture zone of the Gorkha earthquake lies in the western part of our study area. The 7.2 M_w aftershock on May 12th had its epicenter within the Kahule Khola and Bhotekoshi catchment (Roback et al. 2018). In July 2016, the Bhotekoshi and Sunkoshi rivers were affected by a glacial lake outburst flood (GLOF). This event caused extensive erosion far exceeding the typical annual erosion associated with the ISM (Cook et al., 2018). In addition, the flood's impact extended to channel-adjacent hillslopes, where undercutting of riverbanks triggered numerous landslides (Cook et al., 2018).

The Koshi river network drains the full range of lithological units of the Himalayan mountain belt, starting from the Tethyan Sedimentary Sequence in Tibet, through the Higher Himalayan Crystalline, the Lesser Himalayan Crystalline, the Siwaliks, and finally to the alluvial plains of the Gangetic foreland (Schelling, 1992; Nepal, 2016; Sinha et al., 2019; Knight et al., 2024).

Table 2: Overview of hydrologic sampling stations and time of instalment.

	Coordinates	**Elevation**	**Drainage Area**	**Channel Width**	**Upstream Slope**	**Mean annual flow [m^3/s]**	**Distance to the mountain outlet along the channel**	**Sediment Sampling period**	**Grain size measurement period**
Kahule Khola	27.874376N, 85.880545E	1215 m	32 km^2	6 m	12.3 %	Not known	273 km	08.06.2015 – 26.10.2018	10.06.2015 – 20.10.2018
Bhote Koshi	27.79676N, 85.89611 E	873 m	2,400 km^2	30 m	4.1 %	Not known	262 km	08.06.2015 – 31.10.2018	08.06.2015 – 27.10.2018
Sun Koshi	27.338389 N, 85.994373 E	485 m	10,000 km^2	80 m	2.3 %	463	176 km	28.05.2015 – 16.09.2018	01.06.2015 – 16.09.2018
Sapta Koshi	26.868577 N, 87.15221 E	131 m	54,024 km^2	120 m	1.2 %	1289	0 km	18.05.2015 – 28.06.2018	18.05.2015 – 16.12.2017

https://doi.org/10.5194/egusphere-2026-4202
Preprint. Discussion started: 14 August 2026

3 Methods

3.1 Field and Laboratory Analysis

Shortly after the Gorkha Earthquake, and before the monsoon onset in May and June 2015, we installed a network of hydrological stations to sample suspended load at four locations along the Koshi river system (Fig. 1, and Tab. 1). Three litre water surface samples were collected by local partners between 8 and 9 am local time and filtered through a polyethersulfone membrane with a size of 0.22 µm. The rivers were sampled daily during the monsoon seasons 2015 to 2018 and twice a week during the dry seasons. To measure sediment concentrations, the suspended load samples were washed off the filters, dried for 12 to 20 hours at 40 °C and weighed. The dry weight corresponds to the solid fraction of sediment in three litres of river water. For further analysis this was converted to represent gram per litre.

Grain size measurements by laser diffraction, which required < 1 g of material, were performed on subsamples selected to preserve the characteristics of the whole samples. Before the measurements, all subsamples were treated with 10 % solution of H_2O_2 and 10 % HCl for 48 hours to remove any calcium carbonate and organic material. The aliquots were dispersed with sodium pyrophosphate for 24 h and placed in an ultrasonic bath for 15 minutes prior to measurement. Each sample was mechanically disaggregated in the device by ultrasonic excitation for 10 seconds directly prior to measurement. All grain size measurements were conducted by laser diffraction with the Retsch Laser Particle Size Analyzer LA-950. This machine measures 92 classes in a range from 0.011 to 2500 µm. We measured with 2000 sensor acquisitions for each measurement and repeated this 10 times. All counts were converted to volume percent applying the Mie scatter model (Saidi et al., 1995), with a refraction index of 1.55 and an absorption index of 1.33. Finally, we used the mean of 10 consecutive measurements on each sample. In total, we measured 230 samples for the Kahule Khola station, 282 for the Bhotekoshi, 189 for the Sunkoshi, and 219 for the Saptakoshi from June 2015 to October 2018 (data publication: Andermann et al., 2024).

To complement the river samples, we also collected surface sediment samples of several landslide deposits during field campaigns in May-June 2016 and October 2018. We measured the size distribution of grains smaller than 2.5 mm, which is the maximum particle size the Retsch Laser Particle Size Analyzer LA-950 can measure, following the same procedure as used for suspended sediment samples. Moreover, channel bed deposits of tributaries, deposited during floods and exposed during low flows, and debris flow channels were sampled. A total of 28 landslide, 10 debris flow, and 15 tributary deposit samples have been collected.

Discharge data for the stations Sunkoshi and Saptakoshi were provided by the Department of Hydrology and Meteorology of Nepal. Combined with obtained sediment concentrations, discharge data were used to calculate total sediment loads for these two stations. No discharge measurements are available for Kahule Khola and Bhotekoshi.

https://doi.org/10.5194/egusphere-2026-4202
Preprint. Discussion started: 14 August 2026

3.2 End-Member Modelling Analysis (EMMAgeo)

To identify dominant signals from a mixture of several sediment sources, we used the end-member modeling approach implemented in the R package EMMAgeo (Dietze & Dietze, 2019a, 2019b). This algorithm extracts statistically meaningful end-members of a data set using eigenspace analysis. Each end-member is a purely mathematical entity that can be interpreted as one subpopulation in a mixed data set. Together all subpopulations and their sample specific mixing ratios represent the entire data set. An end-member is thus represented by a grain size distribution (loading) and its contribution to each sample (scores). EMMAgeo uses all available mixed sediment samples to identify the unknown grain size distributions (loadings) and individual contributions of end-members to each sample (scores) of the measured data set.

We applied the compact robust protocol (Dietze & Dietze, 2019a) separately to each hydrological sampling station and sediment source type dataset. In other words, end-member modelling was performed independently for each sampling station and sediment source type. We selected the robust protocol because the number of underlying grain-size subpopulations was unknown. This approach facilitates the identification of statistically robust and reproducible end-member structures within the dataset (Dietze & Dietze, 2019a).

As initial step the weight of transformation limits (parameter *l*) were optimised with a dedicated function (get.l). The minimum value of *l* is set to 0 by default, whereas the maximum value is defined as the largest *l* for which eigenspace calculation remains possible. This value is determined either by testing eigenspace computation across a sequence of candidate *l* values or through an iterative approximation of the highest feasible *l* (Dietze & Dietze, 2019a, 2019b). This step is followed by determining a range of possible end-members running the function get.q. This evaluates the proportion of data variance explained by a given number of end-members prior to eigenspace rotation (Dietze & Dietze, 2019a, 2019b). Using these parameters multiple end-member scenarios were calculated (function model.EM). A kernel density estimates from all modelled main grain size modes was used to identify the number of end-members (for details regarding the end-member scenarios refer to the supplementary material). The final step involved using mode limits identified from the kernel density distributions of peak positions across all model scenarios to determine the robust end-members with the function robust.EM (Dietze & Dietze, 2019a, 2019b). In other words, the final number of end-members were selected based on a combination of explained variance and the stability of end-member modes across model scenarios. Fundamentally, the matrix of measured data (**X**), consisting of *m* grain-size distributions (rows), each described by *n* grain-size classes (columns), is used to generate a modelled dataset (**X′**). This modelled dataset is represented as a linear combination of end-member loadings (**V**) and end-member scores (**M**) and reproduces the observed dataset subject to a residual error matrix (**E**). The relationship can be expressed as: $X' = MV^T = X - E$ (Dietze & Dietze, 2019a, Dietze et al., 2022).

We applied the same steps as outlined above to every grain size data set of every sampling station and sediment source type, except for the Bhotekoshi data set, where the maximum and minimum number of end-members needed to be fixed to 2 and 8 classes respectively as the robust protocol yielded an unrealistic maximum of 3 end-members (Dietze & Dietze, 2019a). The

https://doi.org/10.5194/egusphere-2026-4202
Preprint. Discussion started: 14 August 2026

resulting single end-members were interpreted as proxies for specific sediment supply sources. As the grain size distributions of sediment sources were multi-modal, we also applied the end-member modelling analysis to each source type to extract the dominant grain size components following the same steps as outlined above.

Using the modelled relative contribution of each end-member to each sample, we combined these proportions with measured sediment concentrations to calculate end-member-specific sediment concentrations, hereafter referred to as end-member concentrations. For the Sunkoshi and Saptakoshi stations, we additionally calculated end-member-specific total sediment loads, hereafter referred to as end-member total loads.

4 Results

In this section we present results from the end-member modelling for each station and sediment source type. Additionally, we built timeseries of water discharge and sediment flux (for Sunkoshi and Saptakoshi) as well as grain size distributions for all stations. Grain size data timeseries will be presented for each station separately presenting raw grain size data, D_{50} and D_{90} values, and temporal distribution of EM4. Finally, we present seasonal changes of all end-member distributions at each station.

4.1 End-member modelling

The end-member modelling analysis of all grain size data from 2015 to 2018 identified four end-members at the Kahule Khola, headwater catchment and five end-members at main stem the Bhotekoshi, Sunkoshi, and Saptakoshi stations (Fig. 2). Most of the end-members (EM) showed two modes, one of which dominates with an amplitude at least a factor five larger than the next-largest peak. Comparable end-members to the Kahule Khola station also occurred at the downstream stations, with a maximum mode difference of 150 µm (Fig. 2). The Bhotekoshi, Sunkoshi, and Saptakoshi data featured an additional end-member that is coarser than the four end-members of the Kahule Khola. The coarsest end-member at Bhotekoshi and Saptakoshi featured a mode at a grain size between 900 to 1000 µm. At Saptakoshi, the coarsest end-member peaked at about 500 µm and is therefore closer to end-member 4 (EM4) at Sunkoshi, Bhotekoshi, and Kahule Khola with 400 to 450 µm. Overall, the end-member distributions at Saptakoshi showed less distinctive signals, as the distributions of single end-members are more overlapping than those from the upstream stations (Fig. 2).

https://doi.org/10.5194/egusphere-2026-4202
Preprint. Discussion started: 14 August 2026

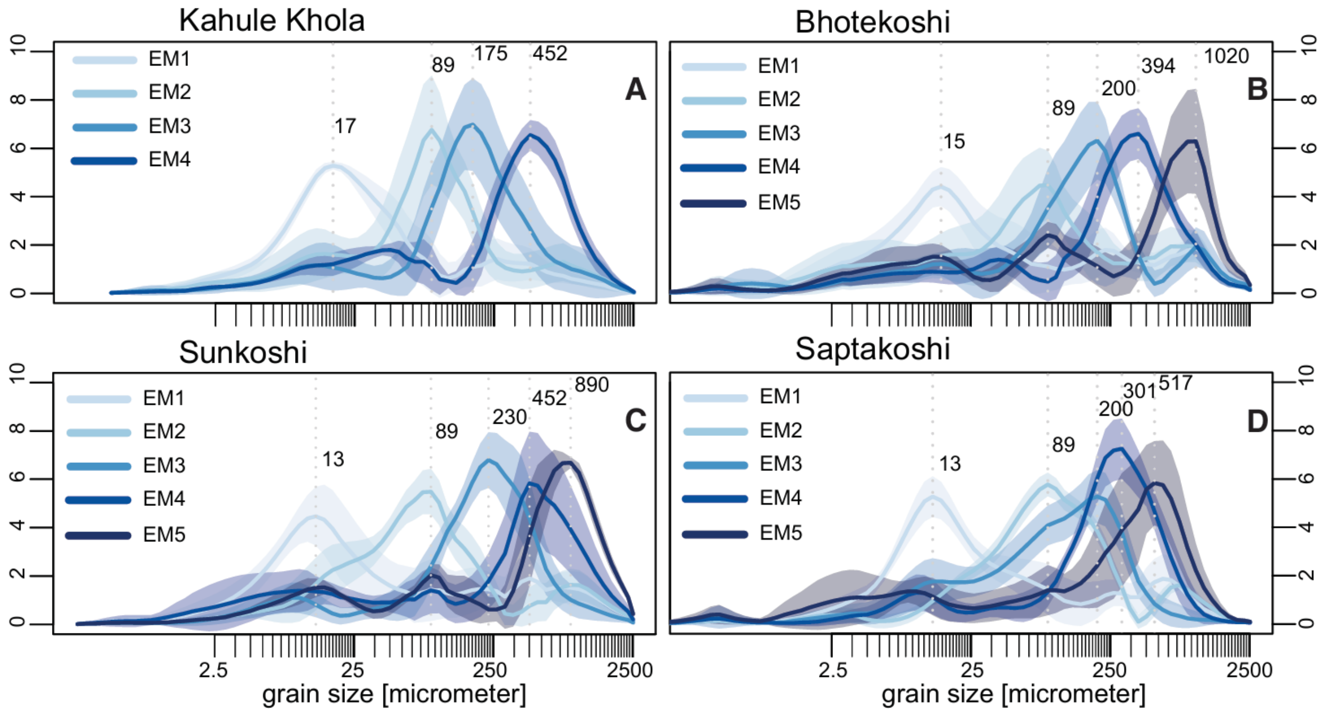

Figure 2: End-member loadings for all four sampling stations. End-member grain size distribution of all respective end-members are shown for data sets of each station. Colouring goes form light blue to dark blue from end-member 1 upward. Peak grain size values of all end-members are written in micrometres. Note a logarithmic scale on the x-axis. Mean sample wise, mean grain size class wise, and mean total explained variance are 0.90, 0.65, 0.77 for Kahule Khola, 0.79, 0.62, 0.70 for Bhotekoshi, 0.87, 0.69, 0.78 for Sunkoshi, and 0.90, 0.55, 0.72 for Saptakoshi (Dietze and Dietze, 2019a).

The landslide GSDs yield similar end-member distributions, with the addition of one coarser end-member in the 2018 samples. Debris flow and tributary deposits gave three end-members, with peak values at 19-44 µm, 229 µm, and 890-1019 µm. Overall, the finest end-member and the coarsest end-member of all samples showed similar peak values as the fluvial sediments. Only the intermediate coarse EM3 is different in the landslides, where the peak value is at 344-592 µm, in comparison to the debris flow and tributary deposits, where the peak value is at about 229 µm (Fig. 3).

https://doi.org/10.5194/egusphere-2026-4202
Preprint. Discussion started: 14 August 2026

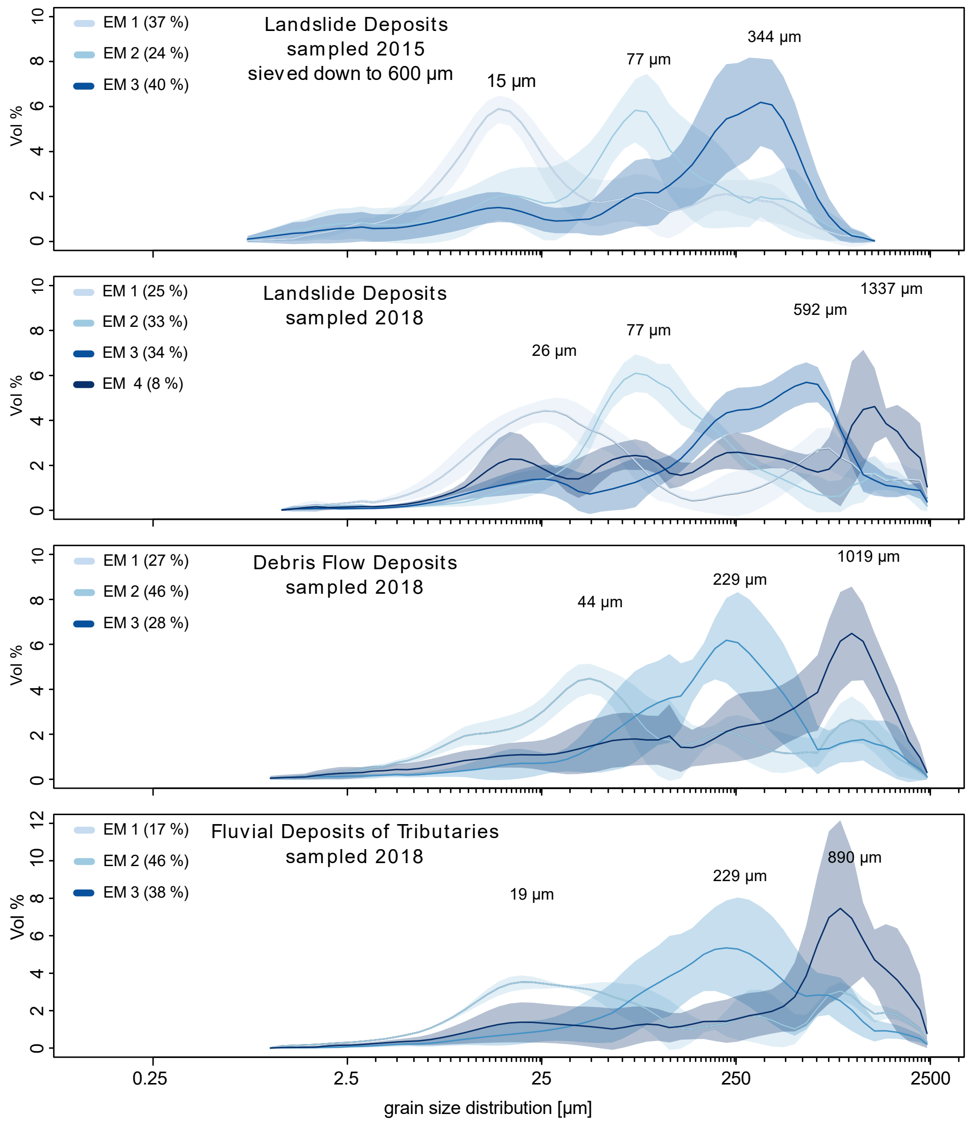

Figure 3: Grain size distribution of end-member signals of possible sediment supply sources. Landslide samples from 2015 were sieved down to 600 µm in the field. The same end-member unmixing approach as for the fluvial sediments were applied to split the grain size distributions into distinctive end-member signals. Color goes from light to dark blue, starting with end-member 1 and upwards. Peak values
265 of all end-member distributions are written into the plots as micrometers.

https://doi.org/10.5194/egusphere-2026-4202
Preprint. Discussion started: 14 August 2026

4.2 Discharge and sediment fluxes time series

Below are discharge and sediment flux time series for Sunkoshi and Saptakoshi some of data has already presented in different in Knight et al. (2024) (data is publish in Andermann et al., 2024). Both station show 2-3 orders of magnitude difference of discharge and sediment flux during monsoon seasons relative to the monitored dry seasons (Fig. 4). We expect the same response for the Kahule Khola and Bhotekoshi, but no discharge data are available. Peak discharges were recorded in July 2018 with 2,370 m^3/s at Sunkoshi, and in August 2018 with 6,990 m^3/s at Saptakoshi. Peak sediment flux was observed on July 6th, 2016, right after the GLOF exhibiting 45,800 kg/s at Sunkoshi. While peak sediment flux at Saptakoshi of 23,000 kg/s was observed on September 1st, 2015.

Mean discharge during monsoon seasons varies for both stations, but lowest mean ISM discharge was observed in 2015 for both stations throughout the observation period. In contrast, highest mean ISM sediment flux was observed in 2015 at both stations (Fig. 4). Subsequent monsoon seasons exhibited a 30% to 46% reduction in mean sediment flux at Sunkoshi and a 30% to 68% reduction at Saptakoshi.

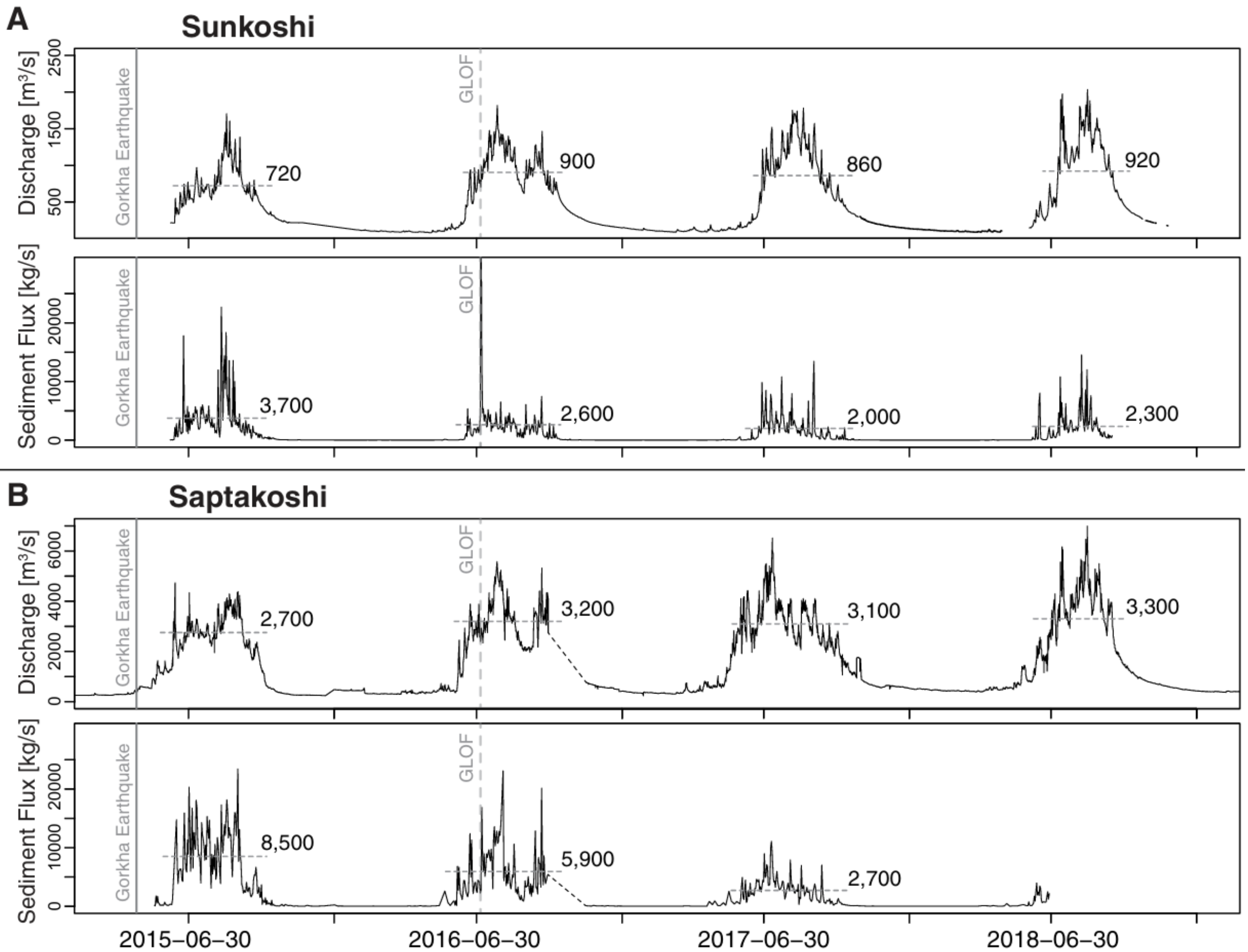

https://doi.org/10.5194/egusphere-2026-4202
Preprint. Discussion started: 14 August 2026

Figure 4: Water discharge and sediment flux time series for the hydrologic stations Sunkoshi (A) and Saptakoshi (B) are shown in this figure. Please note differences in the y-axes scales. Also note some missing data at Saptakoshi time series at the end of the monsoon 2016, indicated with a dashed line. The unusually large peak in sediment flux at Sunkoshi sampling station in July 2016 is from a glacial outburst flood in the Bhotekoshi (Cook et al., 2018). Average discharge and sediment flux values are denoted for all observed monsoon periods.

4.3 Grain size distribution time series

In the following sections we describe temporal changes of grain size distribution of suspended sediments for all sampling stations. This is illustrated by the raw grain size distributions as heat plots, D_{50} and D_{90} metrics, and EM4. The temporal distributions of all remaining end-members at each station can be found in the supplementary material.

4.3.1 Kahule Khola

Suspended sediments at the Kahule Khola were predominantly coarse-grained during the 2015 ISM. Peak grain sizes in the latter half of the monsoon appear higher than those observed earlier in the season. In subsequent seasons, peak grain size distributions varied. Overall, no clear pattern is evident in the raw grain size distribution time series (Fig. 5).

D_{50} and D_{90} values were generally coarser during the 2015 ISM than in 2016 (Fig. 5). However, both metrics increased again in 2017 and 2018, reaching levels comparable to or exceeding those observed in 2015 (Fig. 5). Mean D_{50} values for the ISMs 2015 to 2018 were 70 µm, 69 µm, 115 µm, and 112 µm, respectively, while mean D_{90} values were 251 µm, 201 µm, 331 µm, and 295 µm. During the dry seasons, D_{50} and D_{90} values were not consistently finer than during the monsoon. Isolated high values occurred at the beginning of the 2015/16 dry season and toward the end of 2016/17. The maximum recorded D_{50} was 344 µm, and the maximum D_{90} was 1168 µm, observed on October 13 and 14, 2017, respectively. However, dry-season conditions are represented by relatively few measurements at the Kahule Khola.

At Kahule Khola, EM4 appeared episodically during the 2015 ISM, occurring in 17 of 99 samples (Fig. 5). Despite this, its overall fractional contribution across all end-members was 4.8 %. During the 2016 ISM, EM4 appeared in 2 of 55 samples; in 2017, it occurred in 4 of 19 samples; and in 2018, in 2 of 16 samples (Fig. 5).

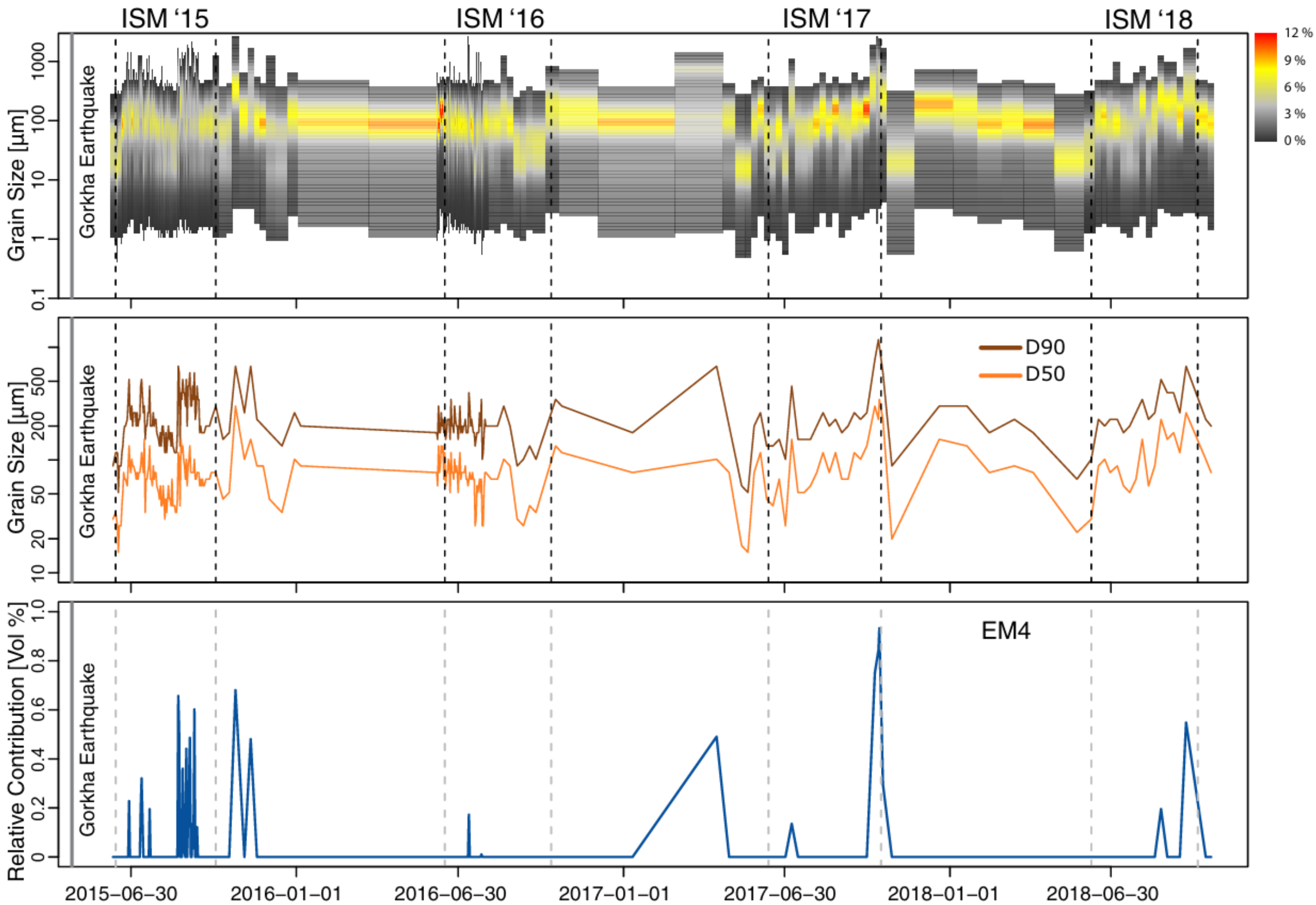

Figure 5: Grain size time series at Kahule Khola. The top panel shows grain size fractions expressed as heat plots, where high shares in certain grain size ranges, peaks in the distribution, are displayed in warm colours. Vice versa, low shares are represented in dark colours. Data density is low for Kahule Khola during dry seasons and is therefore only represented by a low number of data points A none-extrapolated version of this heat plot can be found in the supplementary material. The middle panel shows D_{90} and D_{50} values based on the grain size distribution. The lower panel shows the temporal distribution of EM4.

4.3.2 Bhotekoshi

Suspended sediment in the Bhotekoshi exhibited predominantly coarse grain size distributions, with a nearly constant peak value during the 2015 ISM (Fig. 6). In contrast, the 2016 and 2017 monsoon seasons showed greater variability in peak values. The D_{90} and D_{50} time series (Fig. 6) showed a median value of 412 and 122 µm, respectively, during the 2015 ISM for the Bhotekoshi station. Afterwards D_{90} and D_{50} remained at an almost constant level with a median D_{90} of 241 and a D_{50} of 72 µm, despite unusually high values in January/February 2016 and at the beginning of the monsoon 2016 compared to the entire time series (Fig. 6).

https://doi.org/10.5194/egusphere-2026-4202
Preprint. Discussion started: 14 August 2026

EM4 showed consistent dominance during the 2015 monsoon, with a fractional contribution of 52% and occurrences in 90 of 105 samples. In the remainder of the time series, EM4 appeared only as isolated peaks, primarily during monsoon seasons, contributing just 8% overall. Specifically, EM4 was present in 6 of 50 samples during the 2016 ISM, 3 of 18 samples in 2017, and 5 of 17 samples in 2018. Notably, EM4 peaked on July 5, 2016, coinciding with a GLOF event (Cook et al., 2018).

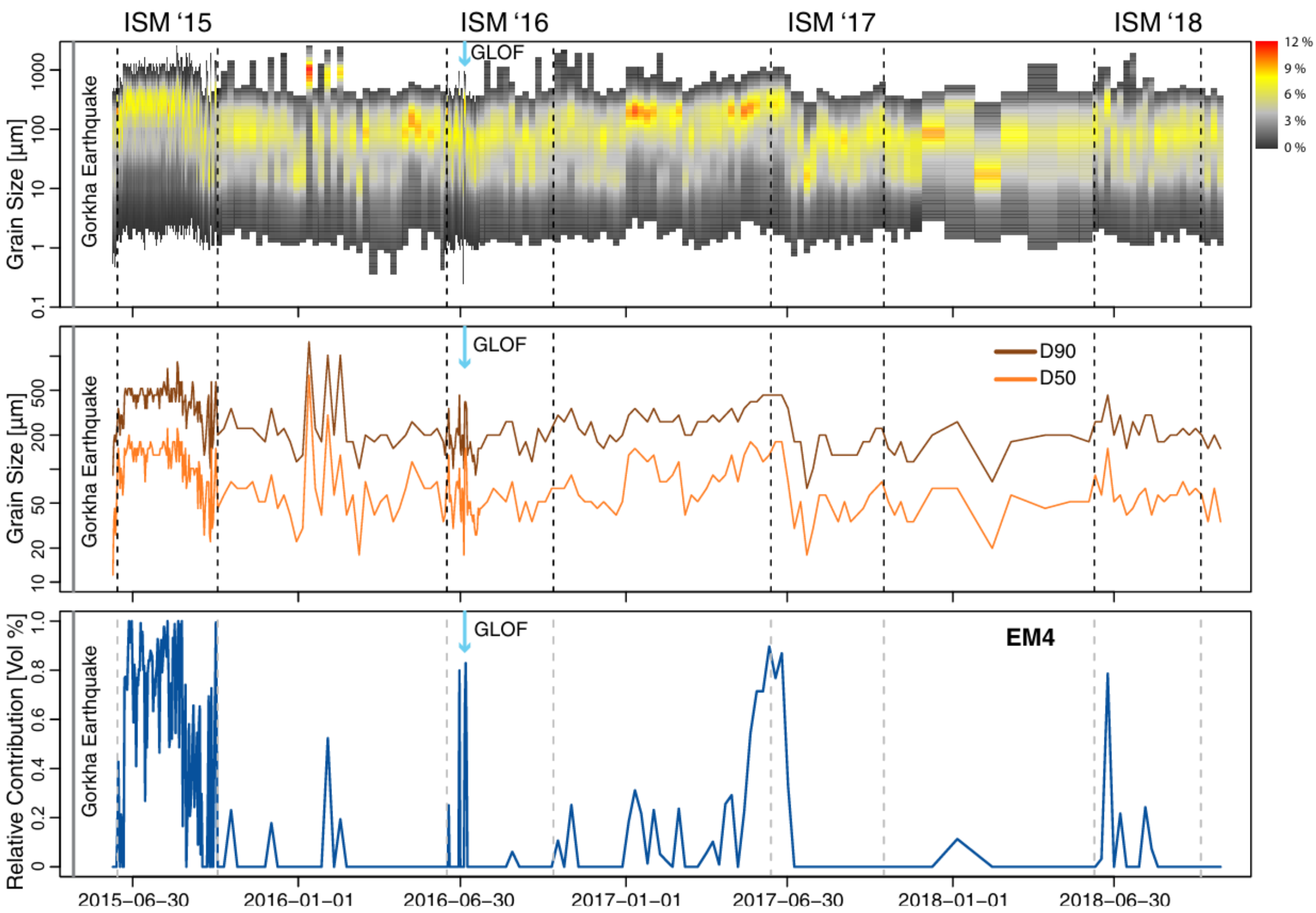

Figure 6: Grain size time series at Bhotekoshi**.** The top panel shows grain size fractions expressed as heat plots, where high shares in certain grain size ranges, peaks in the distribution, are displayed in warm colours. Vice versa, low shares are represented in dark colours. Data is based on daily suspended sediment samples, while in winter seasons samples are extrapolated due to lower sampling density. The middle panel shows D90 and D50 values based on the grain size distribution. The lower panel shows temporal distribution of EM4.

https://doi.org/10.5194/egusphere-2026-4202
Preprint. Discussion started: 14 August 2026

4.3.3 Sunkoshi

Grain size distributions show considerable variability in the Sunkoshi time series. The highest peak values are generally observed during the 2015/16 dry season (Fig. 7). The post-earthquake 2015 ISM does not exhibit a markedly different signature compared to subsequent seasons (Fig. 7).

Grain size distributions did not show elevated D_{50} or D_{90} values during the 2015 monsoon. Instead, the highest D_{50} and D_{90} values were recorded in November 2015 (Fig. 7). In general, the 2015/16 and 2016/17 dry seasons exhibited higher D_{50} and D_{90} values than the preceding monsoons. In contrast, the 2017/18 dry season showed lower D_{50} and D_{90} values than the 2017 ISM (Fig. 7).

EM4 showed minimal presence in the Sunkoshi dataset throughout the observation period. It was absent during the 2015 ISM, followed by a few isolated occurrences in the 2015/16 dry season. Only single occurrences were recorded during the 2016 and 2017 ISMs, each with minimal fractional contributions to the respective samples (Fig. 7).

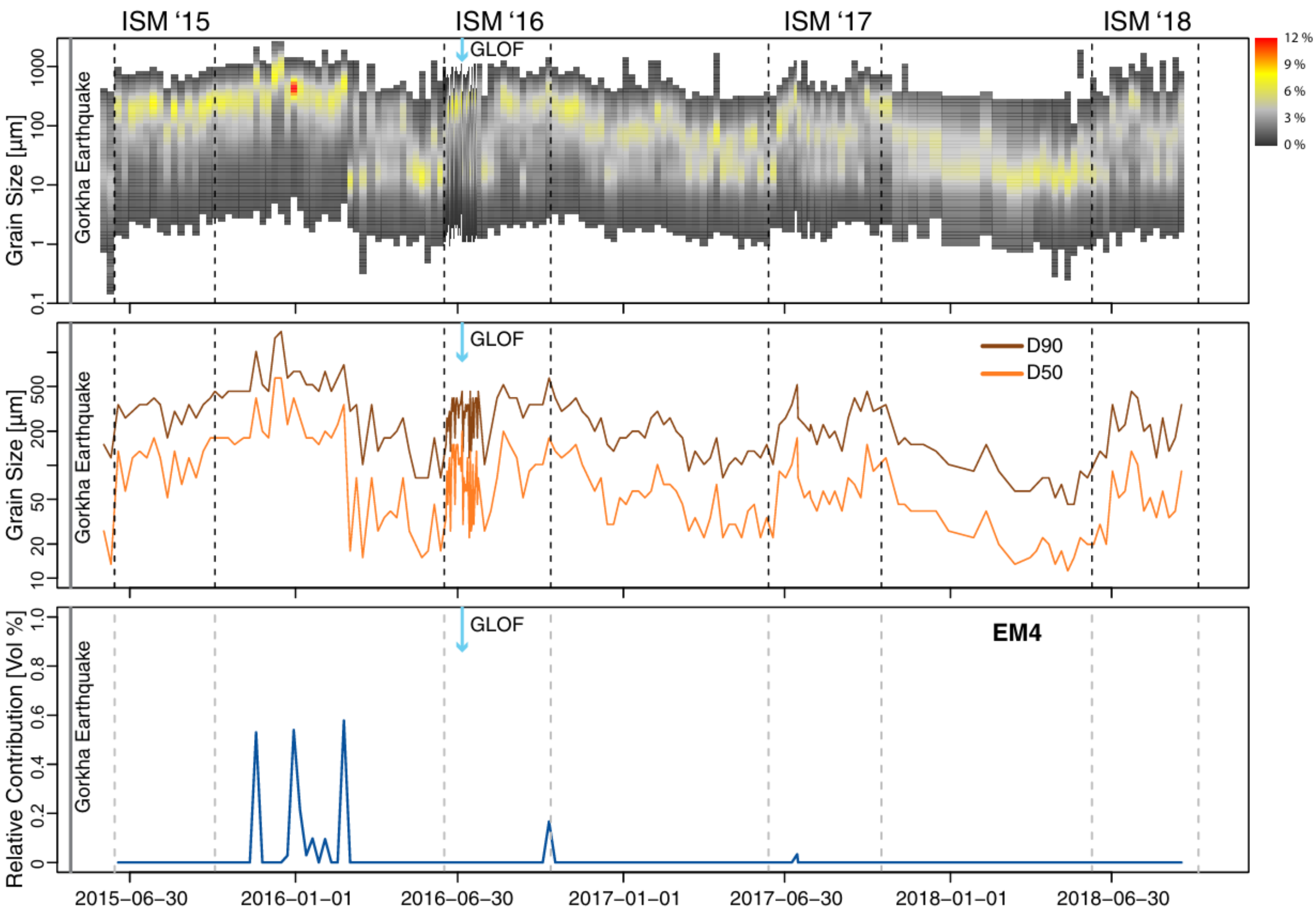

Figure 7: Grain size time series at Sunkoshi. The top panel shows grain size fractions expressed as heat plot. The middle panel shows D_{90} and D_{50} values based on the respective grain size distribution. The lower panel shows temporal distribution of EM4.

https://doi.org/10.5194/egusphere-2026-4202
Preprint. Discussion started: 14 August 2026

4.3.4 Saptakoshi

Grain size distributions show somewhat pronounced peaks during the 2015/16 dry season in the Saptakoshi time series. In general, the distributions appear more multimodal compared to upstream stations. Overall, grain size distributions varied considerably throughout the observation period. Dry seasons tend to exhibit coarser peak values than the ISMs (Fig. 8).

As observed in the Sunkoshi dataset, D_{50} and D_{90} time series did not show elevated values during the 2015 monsoon (Fig. 8). Instead, the highest D_{50} and D_{90} values were recorded during the dry seasons. Mean D_{50} values during the ISMs ranged from 51 to 110 µm, while mean D_{90} values ranged from 255 to 344 µm. In contrast, the 2015/16 dry season exhibited a mean D_{50} of 151 µm and a mean D_{90} of 495 µm. Similarly, the 2016/17 dry season showed mean D_{50} and D_{90} values of 128 µm and 470 µm, respectively.

EM4 at the Saptakoshi represented 30% contribution to the entire time series with appearance in the monsoon season 2015 (30%) and otherwise mainly during the dry seasons (40% to 30%) (Fig. 8).

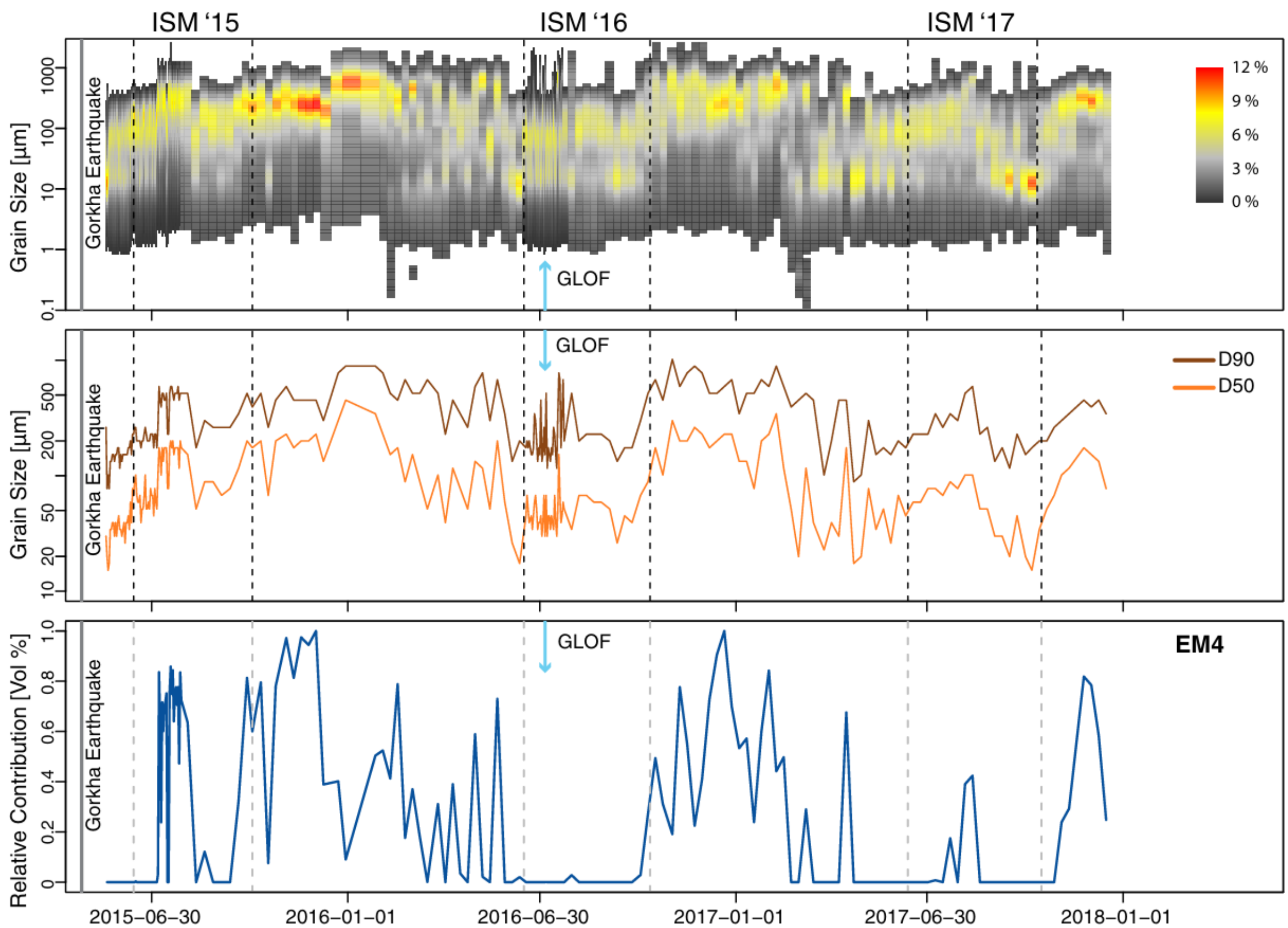

Figure 8: Grain size time series at Saptakoshi. The top panel shows grain size fractions expressed as heat plot. The middle panel shows D90 and D50 values based on the grain size distribution. The lower panel shows temporal distribution of EM4.

4.4 Seasonal changes of end-member distributions

The following section describes changes in average seasonal end-member distributions between monsoon and dry seasons. We examine (i) shifts in relative end-member distributions, (ii) changes in end-member concentrations, and, for the Sunkoshi and Saptakoshi, (iii) changes in total end-member load distributions. The description proceeds from upstream to downstream sampling stations, comparing ISMs and dry seasons separately.

Relative distribution of the end-members for the monsoon seasons 2015, 2016 and 2017, as well as for the dry seasons 2015/16, 2016/17, and 2017/18, exhibited different trajectories at every hydrologic station (Fig. 9 and 10). During the post-earthquake monsoon 2015 the coarse end-members tend to show a greater presence than in the following ISMs 2016, 2017, and 2018 (Fig. 9 and 10). This can be observed at each station except Kahule Khola but based on different end-member distributions. Throughout the observed ISMs, at the Kahule Khola, EM4 initially contributes 4.8 % in 2015, in 2016 about 0.3 %, in 2017 about 10 %, and in 2018 about 4.6 %. At the Bhotekoshi, EM4 initially contributes 52 % in 2015, and about 6 % to 7 % in 2016, 2017, and 2018. At the Sunkoshi and the Saptakoshi, EM4 did show minimal presence during the ISMs. However, a continuous reduction of the next coarser EM3 can be observed throughout the observed ISMs. At Sunkoshi the presence of EM3 decreases from 67 % in 2015 to 49 % in 2016, to 30 % in 2017, to eventually 23 % in 2018. However, at Saptakoshi the presence of EM3 initially decreased from 42 % in 2015 to 19 %, in 2016, but increased again in 2017 to 38%.

The relative distributions during the dry seasons did not depict any consistent trend of decreasing or increasing coarseness of fluvial sediments. At the Kahule Khola the observed dry seasons showed comparable relative end-member distributions, while only EM4 during the dry season 2017/18 increased compared to previous dry seasons. At the Bhotekoshi the coarsest EM5 is only present during the 2015/16 dry season with 5 %. EM4 moved from 3 % to 16 % and to 0.7 % from 2015/16 to 2016/17 and to 2017/18. At the Sunkoshi station EM5 only appeared during the dry season 2015/16 and contributed 7 %, while EM4 contributed 4 % during the same season. The remaining dry seasons exhibited 0 % to 0.4 % of EM4. While EM3 decreased from 51 % to 21 %, and to 0 % for the dry seasons 2015/16, 2016/17, and 2017/18 (Fig. 10). At the Saptakoshi stations the end-member distribution for the dry seasons 2015/16 and 2016/17 exhibited a quite comparable pattern with no major reduction or increase of single end-member contributions.

The highest average sediment concentrations occurred during the post-earthquake monsoon 2015 at every station (Fig. 9 and 10). At the same time, we observe a continuous reduction of average concentration over the following monsoon seasons until 2018, except at Kahule Khola, where the concentration in 2017 is comparable as in 2015. The average sediment concentration during the dry seasons was much lower than during the wet seasons, except for the Kahule Khola, where the average

https://doi.org/10.5194/egusphere-2026-4202
Preprint. Discussion started: 14 August 2026

concentration during the dry season 2015/16 is higher (0.41 g/l ± 0.12) than in the ISM 2016 (0.35 g/l ± 0.04) as well as comparable in the ISM 2018.

In the same way as the total average concentrations decrease, we tend to observe that the average concentrations for EM3 or EM4 reduced in greater manner than the average concentrations of EM1 and EM2. However, at Kahule Khola the coarse EM4 was high again in 2017 (about 0.06 ± 0.03 g/l). At the Bhotekoshi station the average concentration of EM4 reduced from 2.2 ± 0.3 g/l in 2015 to 0.2 ± 0.01 g/l in 2018. EM3 at Sunkoshi reduces throughout the ISMs from 2.8 ± 0.5 g/l in 2015 to to 0.3 ± 0.1 g/l in 2018. At Saptakoshi EM3 reduced from 2.0 ± 0.5 g/l to 0.3 ± 0.08 g/l from ISM 2015 to 2017.

Lastly, the total end-member load distribution at Sunkoshi and Saptakoshi exhibited a similar trend of reduction of EM4 and EM3. At Sunkoshi we see predominantly a reduction of EM3, which showed an average flux of 1,991 ± 397 kg/s in 2015 reducing to 371 ± 121 kg/s in 2018. Similarly, at Saptakoshi both EM3 and EM4 decreased rapidly from 6,465 ± 2217 kg/s and 3,240 ± 577 kg/s, respectively, in 2015 to 852 ± 218 kg/s and 12 ± 7 kg/s, respectively, in 2016.

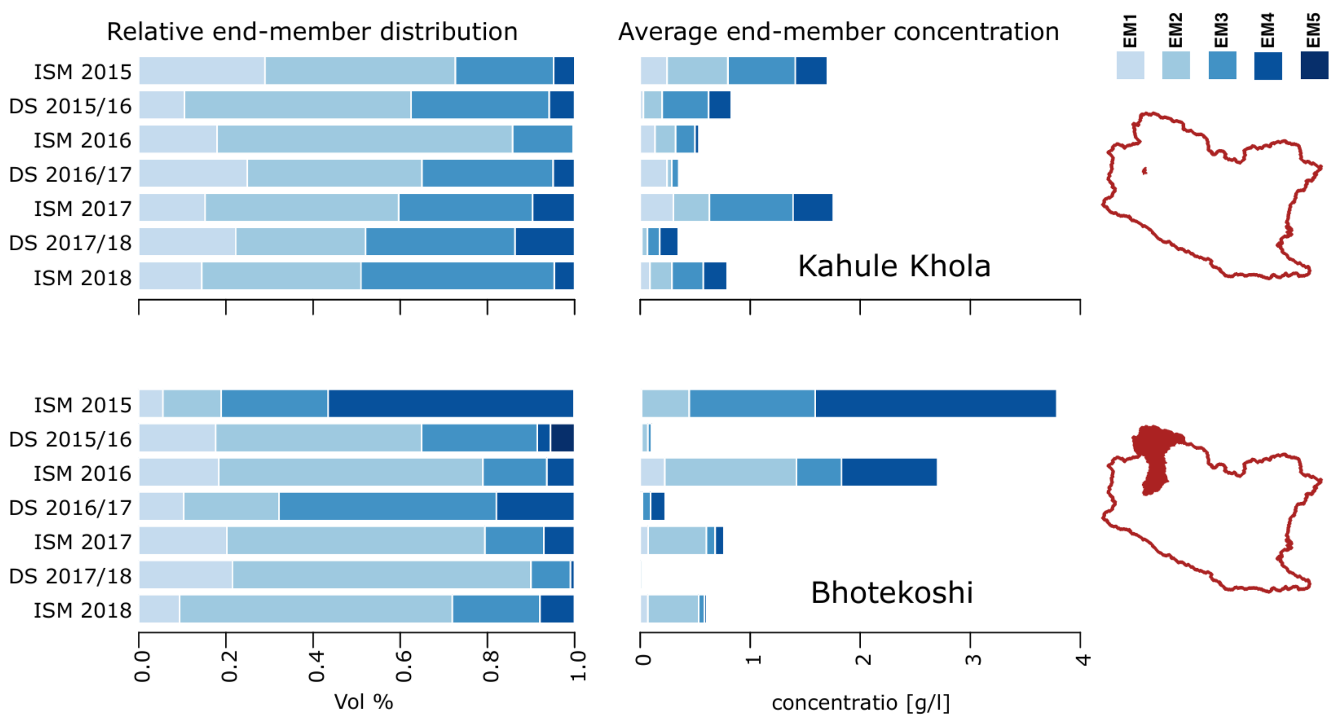

Figure 9: Bar charts for average end-member distribution based on seasons for Kahule Khola and Bhotekoshi. Left side shows relative end-member contribution per season. Right side shows average end-member concentration in g/l per season. Seasons are divided in monsoon (ISM) and dry season (DS), and an average is taken over all samples falling into one season. Inlet overview map to the right shows the location and proportion of the respective drainage basin within the entire nested catchment.

https://doi.org/10.5194/egusphere-2026-4202
Preprint. Discussion started: 14 August 2026

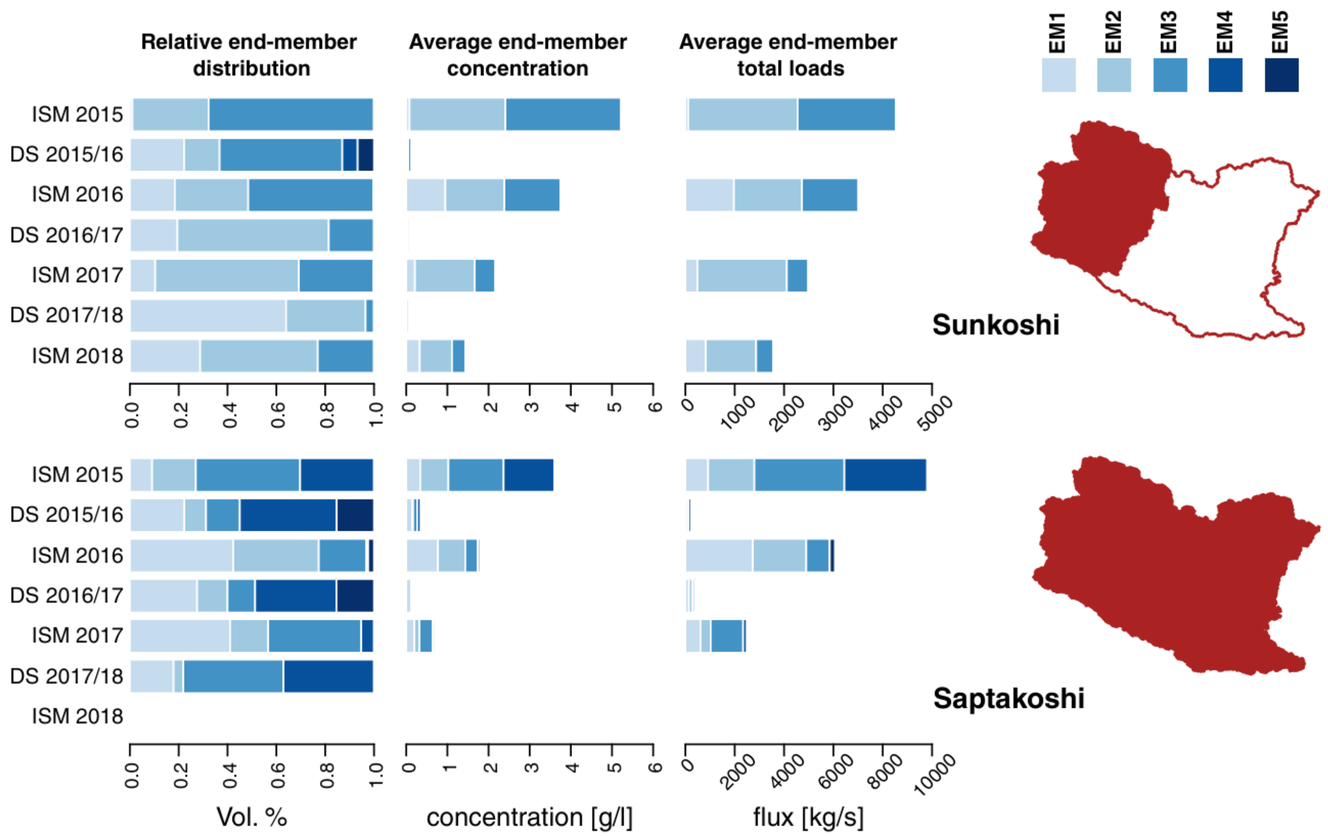

Figure 10: Bar charts for average end-member distribution based on seasons for Sunkoshi and Saptakoshi. Left column shows relative end-member contribution. Middle column shows average end-member concentration in g/l, and right column shows average end-member sediment flux in kg/s. Seasons are divided in monsoon (ISM) and dry season (DS) and an average is taken over all samples falling into one season. Please note that the average sediment flux for Saptakoshi for monsoon 2017 is based on limited samples and is most likely underestimating total sediment flux for this season. Inlet overview map to the right shows the location and proportion of the respective drainage basin within the entire nested catchment.

5 Discussion

5.1 Earthquake-driven grain size signal

The grain size distributions of suspended sediments tend to be coarser within the first monsoon after the Gorkha Earthquake at all stations, except at Kahule Khola, compared to the remaining monsoon seasons of sampling after the event. As the Gorkha Earthquake triggered 2-3 orders of magnitude more landslides than a typical monsoon season (Roback et al. 2018, Marc et al. 2019), this coarseness in suspended sediments probably relates to increased supply of landslide material. Similarly, previous studies observed a relationship between landsliding and coarsening of fluvial sediments (Whittaker et al. 2010, Attal et al. 2015, Struck et al. 2015, East et al. 2018).

https://doi.org/10.5194/egusphere-2026-4202
Preprint. Discussion started: 14 August 2026

At sampling stations Kahule Khola and Bhotekoshi EM4, the coarsest and second coarsest end-member, respectively, showed relatively strong presence during the ISM 2015. This suggests that EM4 might signal mass wasting caused by the Gorkha Eartquake. Particularly, at the Bhotekoshi EM4 showed a total contribution of 55% during the 2015 ISM and little appearance in subsequent monsoon seasons of only 6%, 7%, and 6% in 2016, 2017, and 2018. The pattern is less clear at the Kahule Khola station, where EM4 appears as a series of strong, short-lived events during the 2015 monsoon (Fig. 5), rather than the more continuous occurrence observed at the Bhotekoshi station. Moreover, at Kahule Khola EM4 shows comparable overall presence in 2017 as in 2015, but less frequently than in 2015. Given the small drainage basin size of Kahule Khola (32 km²), it is likely that suspended sediment transport is impacted by highly episodic sediment supply. Reappearance of EM4 in the 2017 could stem from reactivation of 2015 landslide material or new mass movements. There was a minor uptick in landslide density in 2017 compared to 2016 in the Bhotekohshi catchment (Marc et al., 2019), while ISM strength was lower in 2017 compared to 2016 (Department of Hydrology and Meteorology, 2025). The much larger drainage basin of the Bhotekoshi station (2,400 km²) likely buffers the influence of localized events, resulting in a more continuous sediment signal during the 2015 monsoon season.

At the Sunkoshi and Saptakoshi sampling stations, no single end-member can be directly linked to earthquake-induced mass wasting. However, Sunkoshi shows a greater presence of coarse-grained end-members (particularly EM3) during the 2015 monsoon compared to the monsoons from 2016 to 2018. This likely reflects an increased supply of landslide-derived material following the earthquake. Nevertheless, due to the large drainage areas of these stations, a distinct grain-size signal cannot be clearly discerned.

Altogether, a considerable amount of suspended sediment export can be attributed to landsliding in 2015 mostly in drainage basins highly impacted by co- and post-seismic landsliding. However, this attribution relies on the assumption that the ISMs 2016, 2017, and 2018 are representative for pre-earthquake ISMs. This assumption is informed by other studies observing a post-earthquake related signal for increased landsliding (Marc et al., 2019), carbon export (Maerki et al., 2021), and seismic velocity recovery (Illien et al., 2022) only in 2015. After the monsoon 2015, the grain size distribution is not greatly influenced by either the onset of monsoon or dry season (Fig 2 and 3), leaving a unique grain size distribution of suspended sediments in 2015. In other words, the supply through increased landsliding responsible for creating the 2015 signal is not dominant anymore in 2016, 2017, and 2018. Hence, the observed grain size signal might be predominantly a signal of increased sediment production through landsliding (Marc et al., 2019) rather than a continuous evacuation of available sediments in subsequent years. The transient earthquake signal dissipated after 2015 (Illien et al., 2025).

Following our interpretation of the 2015 signal, suspended load in 2016, 2017, and 2018 features a smaller fraction of landslide-supplied material (EM4) than in 2015 most clearly observed in the Bhotekoshi. The earthquake-induced mass wasting debris that reached the channel might have been exported efficiently in 2015. Alternatively, a large volume of sediment mobilized by co- and post-seismic landslide deposits must be still stored on hillslopes or in low-order headwater channels (Pearce & Watson, 1986).

https://doi.org/10.5194/egusphere-2026-4202
Preprint. Discussion started: 14 August 2026

Due to the absence of discharge data, it remains uncertain whether sediment export also returned to pre-earthquake levels within the timeframe of one year. Insights from the Wenchuan 2008 Earthquake indicate elevated bed material export on decadal scales (Li et al., 2025). While sediment flux data from the Sunkoshi station indicate relatively stable rates during the post-earthquake monsoons from 2016 to 2018, whereas the Saptakoshi station shows a continued decline into the 2017 monsoon. Additional background data are needed to better constrain the temporal impact of large earthquakes on sediment export at the mountain outlet in the Himalayas. Particularly bed load information would be valuable to be added in future research. The Bhotekoshi showed negligible increase in coarse-sediment accumulation post-earthquake (Graf et al., 2024), which might allude to poor connectivity of existing landslides material to channels and no increased sediment production after 2015.

Previous studies showed that comparable large earthquakes can affect landsliding and sediment export response for several years (Dadson et al. 2004, Hovius et al. 2011, Wang et al. 2015 Marc et al. 2015, Li et al., 2025), and that the duration of increased supply correlates well with the duration of elevated sediment export (Hovius et al. 2011). In the Koshi basin the fluvial earthquake signal is only present for ~1 year, in agreement with the short duration of elevated post-seismic landsliding and debris flow rates in Nepal, which returned to the pre-earthquake level in 2016 (Marc et al. 2019, Dahlquist and West, 2019, Kincey et al., 2021). Although landslides triggered in 2015 persisted in the landscape for several years likely affecting sediment supply and transport. This, however, did not create a lasting signal beyond the 2015 ISM. Poor transfer of sediment from landslide deposits to channels may explain the short-lived signal. As a large portion of the 2015 landslides exhibit a great distance to the nearest channels (Supplementary Material, S3). Alternatively, the transfer of material from those sources to the channel may take more time than this study covers, or the volume of material coming from those deposits may be insufficient to produce a clear grain size signal as has been observed for 2015. However, many active landslide deposits not connected to channels or in headwater catchments can potentially set the pace for subsequent erosion, because landslide debris might erode slowly in the following years to decades, supplying material to the channels. Also, landslide deposits are susceptible to future mobilization as mass wasting events triggered by intense rain or future seismic shaking (Yanites et al., 2025).

Overall, the Gorkha Earthquake was less destructive than other events with a comparable magnitude (Marc et al. 2016, Xu et al. 2016) in terms of the moderate landslide volume it produced (~0.8 km^3, Roback et al. 2018) and the short recovery period of post-seismic landsliding (~1 year, Marc et al. 2019, Illien et al., 2022). Further, the Gorkha Earthquake had a minor impact on organic carbon export with an 85% increase in 2016 in the Narayani Basin, an adjacent drainage basin to the Koshi basin (Maerki et al. 2021). In contrast, the Wenchuan Earthquake doubled organic carbon export over 4 years in a catchment comparable in terms of basin size and number of co-seismic landslides (Wang et al. 2016). In Nepal, sediment fluxes were elevated for about one year, a shorter period than those in Taiwan and China caused by a similar magnitude earthquake (Hovius, et al. 2011; Wang et al., 2015). The Wenchuan Earthquake triggered more landslides than in Nepal (Wang et al., 2015), which

https://doi.org/10.5194/egusphere-2026-4202
Preprint. Discussion started: 14 August 2026

could explain this difference. However, it remains unclear how differences in landscape characteristics across these geographic settings influence the sediment flux signal induced by an earthquake.

5.2 Linking grain size distribution of sediment sources to fluvial sediments.

The grain size distribution of our empirical reference material, i.e. the surface sample material of landslide deposits, debris flow and tributary deposits show only minor differences in coarseness (Fig. 3). However, landslide deposits show an end-member with a mode at 344 and 529 µm comparable to the mode of EM4 in the suspended sediments, with a total abundance in both landslide grain size data sets of 40 % and 34%, respectively. A comparable end-member cannot be identified in the deposits of debris flows and tributaries. This indicates that subsequent mobilization of landslide material via debris flows or tributaries may not retain the distinct grain size signature of direct landslide input, as grain size sorting and selective transport processes combined with less transport capacity in tributaries compared to main streams can alter sediment characteristics. As the majority of 2015 landslides are within a large distance to channels (Supplementary Material, S3) input after 2015 through secondary mobilization might not create the same grain size signal as in 2015. We interpret the EM4 signal observed at the Kahule Khola and Bhotekoshi in 2015 to primarily reflect landslide material delivery to channels with minimal reworking processes.

Underlying lithology can strongly influence the grain-size distribution in landslide deposits (Attal and Lavé, 2009). In the Kahule Khola and Bhotekoshi catchments, the dominant bedrock types where the majority of landslide occurred are granite and gneiss, and dolomite (Table 1). Deposits derived from granite and gneiss tend to have slightly coarser median grain sizes (D50 = 43–278 µm) than those derived from dolomite (D50 = 27–106 µm) (see supplementary material). However, the wide variability in median grain size within each lithology prevents a clear discrimination of source material as the primary control on grain-size distribution. Moreover, factors such as the degree of fracturing and weathering of the bedrock are also likely to exert a substantial influence on the grain-size distribution of landslide deposits (Marc et al., 2021; Sklar et al., 2020).

5.3 Effect of glacial lake outburst flood on earthquake perturbation

The Bhotekoshi was hit by a glacial lake outburst flood (GLOF) event on the 5th of July during the 2016 monsoon season (Cook et al., 2018). The catastrophic release of a high volume of water into the Bhotekoshi system led to rapid and severe fluvial erosion. Moreover, sustained landsliding of undercut channel toe slopes occurred because of this GLOF. The same EM4 indicating earthquake-induced supply in 2015 also peaked from 05.07.2016 to 07.07.2016 in response to the GLOF (see Fig. 6). We attribute this peak to landslides that remained active after the flood wave had ceased (Cook et al. 2018). The GLOF likely affected the temporal development of an earthquake response signal by again perturbing the system. The flood might have washed out the coarse earthquake-derived sediments, which otherwise would have created a signal spread over the monsoon 2016 period. Conversely, the Ghorka earthquake could have affected the channel response to the GLOF. Hillslopes

https://doi.org/10.5194/egusphere-2026-4202
Preprint. Discussion started: 14 August 2026

weakened by a recent earthquake may be more prone to flood-induced, toe-cut landsliding (Larsen & Montgomery, 2012, Yanites et al., 2025). These different effects are potentially important but cannot be resolved with our data. As a consequence, the temporal proximity of earthquake perturbation to GLOF perturbation could mean that we underestimate the recovery time of the Gorkha Earthquake.

5.4 Downstream propagation of earthquake grain size signal

Seasonal averages of end-member composition show that suspended sediments were coarser during the 2015 ISM compared to subsequent ISMs at Bhotekoshi, Sunkoshi, and Saptakoshi. While at Kahule Khola the 2017 and 2018 ISMs also show relative coarse end-member distributions. Both the Sunkoshi and Saptakoshi stations also exhibit increased sediment coarseness during the winters of 2015/16 and 2016/17. There is an individual earthquake related end-member signal detectable at Bhotekoshi, which disappeared within ~100 km downstream to the Sunkoshi station. Due to the nested catchment approach, the drainage areas increase substantially after each station, and the co-seismic landslides are concentrated in a small portion of the Koshi basin (Fig. 1). The portion of each drainage basin affected by landsliding is comparable in the Bhotekoshi and Sunkoshi basins at 0.5% and 0.4%, respectively. But the median travel distance of landslide deposits to the Sunkoshi sampling station is much greater than to the Bhotekoshi station. Hence, there is a high chance of a signal dilution, which in this context means that the grain size signal created upstream increasingly disappears downstream because of numerous other processes contributing to the sediment load like abrasion, soil erosion, or reworked terraces. This makes it overall harder to detect individual end-member signals in the downstream stations Sunkoshi and Saptakoshi compared to the upstream stations Kahule Khola and Bhotekoshi. However, at Sunkoshi a continuous reduction of EM3 through the ISMs 2015 to 2018 can be observed. This alludes to decreasing coarseness of suspended sediments, but without producing a clear end-member signal.

After their generation, sedimentary signals travel through a transfer zone before they reach their sink (Romans et al. 2016). It is unclear where the earthquake-generated suspended sediments are deposited. If a sedimentary archive is formed upstream of the Bhotekoshi station it might record an earthquake signal as a distinct end-member in the grain size distribution (Schwanghart et al. 2015). Downstream of the Sunkoshi station a potential archive might record only unusual coarse sediments for a monsoon season, which is likely not sufficient to identify an earthquake. Flooding can also lead to a coarsening of fluvial sediments, which complicates the distinction between flood- and earthquake-driven sediment signatures in the sedimentary record. Despite this, our study offers valuable process-based and quantitative insights into the temporal and spatial patterns of suspended sediment grain size distribution in response to shifts in sediment supply caused by co-seismic mass wasting. Although our approach reveals the post-seismic response of fluvial suspended sediment systems, it remains unclear how bedload transport responds and whether it can be applied to archives that contain a mix of suspended and bedload sediments.

https://doi.org/10.5194/egusphere-2026-4202
Preprint. Discussion started: 14 August 2026

5.5 Implications and limitations

Major earthquakes can trigger a pulse of hillslope erosion and are therefore an important driver of mountain landscape evolution (Parker et al. 2011, Li et al. 2014 & 2016, Marc et al. 2016). We show that widespread co- and post-seismic mass wasting can alter the characteristics of suspended sediments in rivers draining landslide affected catchments. Although the net volume of exported sediment might be small compared to total mass wasted volumes during our study period, the difference in grain size distribution of suspended sediments allows one to trace it for a whole monsoon season. This may produce a signal that could be interpreted as evidence of paleo-earthquakes; however, it remains unknown whether floods and earthquakes generate similar grain size signatures. Paleo co- and post-seismic sedimentation rates have already been successfully estimated from lake sediments in New Zealand (Howarth et al. 2012). Similar insights could be achieved by studying archives built on terraces or local deposits like lakes in other seismically active regions. Zhang et al. (2019) made a direct link between seismically induced mass wasting and its translation into sedimentary records after the Wenchuan Earthquake 2008, observing increased D_{50} in sedimentary archives within a few years of the earthquake. Preserved granulometric proxies of widespread co-seismic mass wasting can give estimates of post-seismic sedimentation rates. The Gorkha Earthquake's impact on grain size distribution throughout an entire monsoon season, mainly near landslide-affected areas, provides valuable process-based evidence of how changes in sediment supply patterns influence the grain size distribution of fluvial sediments.

The return periods for large earthquakes in the Himalayas remains debated, especially in western Nepal and northern India. The last known major earthquake in western Nepal was the M_w ~8.2 earthquake of 1505 AD (Kumar et al. 2006). The lack of a major event in the last ~500 years led to the concept of a seismic gap in western Nepal. However, historical and paleo-seismic records of earthquakes are notoriously incomplete (Bollinger et al. 2016, Bilham 2004). Analysis of lake turbidites revealed more earthquakes than generally assumed in this area, challenging the prevailing theory of a seismic gap (Ghazoui et al. 2019). Grain size-specific signals linked to earthquake-induced increases in landsliding recorded in fluvial archives may offer a means to identify paleo-earthquakes. However, this depends on developing a stronger process-based understanding of how or if such signals are preserved, and how they can be distinguished from those produced by other disturbances, such as major floods.

Beyond paleoenvironmental reconstructions, our findings indicate usefulness in linking signals derived from grain size distribution to supply sources. Grain size distribution analysis could be a cost- and time-effective alternative to, for example, geochemical sediment fingerprinting (Haddadchi et al. 2013). Our results indicate that major perturbations in supply patterns like earthquakes might create their own end-member within grain size distribution of suspended sediments. Similarly, to the idea that different grain sizes can carry different age information (Lukens et al., 2023). However, this requires a better understanding of how grain size signals are connected to lithology, weathering rates, climate, biota, and erosional processes (Sklar et al. 2017), as well as how well signals from different supply sources are transferred to channels. Additionally, the interaction between bedload and suspended load and whether both are captured in the stratigraphic record will complicate the

https://doi.org/10.5194/egusphere-2026-4202
Preprint. Discussion started: 14 August 2026

applicability of this method. Nevertheless, our results represent a step toward a quantitative understanding of how sediment supply processes influence the grain size distribution of fluvial sediments. Further research is required to determine whether these signals are reliably preserved in sedimentary archives.

One of the main limitations of our study is that we have only sampled suspended sediments close to the water surface at the thalweg. Generally, it is assumed that coarse suspended grains migrate deep within the water column and therefore may not be easily sampled from the surface. Due to the high turbulence in the upstream rivers, this limitation might be less of a concern for sediments from Kahule Khola and Bhotekoshi stations but can influence grain size variability in the suspended sediments from the downstream stations of Sunkohsi and Saptakoshi (Dingle et al. 2020). Thus, it is possible that our grain size data set underestimates the coarseness of some of the suspended sediments or, vice versa, the relative contribution of given end-members. However, Morin et al. (2018) showed with vertical profiles of suspended sediment concentration and grain size distribution sampled along the Narayani River that this effect is negligible. Finally, possible natural or anthropogenic sinks such as lakes, dams, and constrictions, can be expected to affect grain size characteristics, which require future studies for better constraints.

Suspended sediment characteristics are also influenced by hydrologic parameters. Unfortunately, discharge data are only available for the downstream stations at Sunkoshi and Saptakoshi. At Sunkoshi, sediment rating curves suggest that by the end of the observation period in 2018, high flows transport slightly less suspended sediment than in previous years (Supplementary Material, S4). This change may reflect greater sediment availability in the immediate post-earthquake years. In contrast, no similar trend is observed at Saptakoshi. Overall, we assume that suspended sediment export at the upstream stations is strongly influenced by sediment supply, as also reported by Andermann et al. (2012). However, no direct relationship with hydrologic forcing can be demonstrated. Additionally, due to limited data, we cannot reliably assess how changes in transport mode, such as the movement of coarse grains as bedload during low flows, affect suspended load grain size distributions. This limitation complicates a direct, linear relationship between grain size characteristics and sediment supply.

6 Conclusion

The Gorkha Earthquake likely affected the characteristics of suspended sediments in the Koshi basin during the subsequent monsoon season. The texture of the suspended sediments is affected from the headwater streams to the mountain front 150 km further downstream. Upstream at the Kahule Khola and Bhotekoshi a single end-member could be identified that likely related to the earthquake-driven hillslope supply. Increased coarseness can also be observed at the downstream stations Sunkoshi and Saptakoshi, where it was not possible to identify a single end-member related to earthquake-associated mass wasting, likely because the signal is diluted with increasing catchment size and downstream travel distance. The grain size response is visible for the monsoon season 2015 but becomes increasingly difficult to identify in the subsequent years 2016, 2017 and 2018. This implies that material contributed by landsliding directly to the river channels was excavated efficiently by the fluvial network during one monsoon season.

These findings provide novel process-based evidence of how sediment supply influences the grain-size distribution of fluvial sediments. Grain-size records in sedimentary archives are commonly used to infer environmental changes and major perturbations such as earthquakes and floods, yet they are often interpreted with limited process-based understanding of how such signals are created, transported, and preserved. Our study highlights the complexity and challenges of tracing earthquake-induced grain-size signals in suspended sediments. Lithology, hydrology, and transport dynamics all shape sediment texture, complicating the persistence of source-derived signals. Although only at the upstream stations of our sampling network, a distinct grain-size signal attributable to the Gorkha Earthquake is apparent, our results demonstrate the potential of grain-size time series to disentangle sediment supply processes. Expanding such analyses could improve quantitative assessments of the relative contributions of different sediment sources to overall sediment loads and clarify the spatial and temporal scales over which these signals can be detected.

Data availability

The suspended sediment grain size time series have been published in a data publication Andermann et al. (2024). Grain size measurements of landslide deposits and other sediment sources can be access at https://doi.org/10.5281/zenodo.17546956 (Puhl et al., 2025). Discharge data for stations Sunkoshi and Saptakoshi have been provided by the Department of Hydrology and Meteorology, Nepal.

Author contributions

DP designed the study, analysed the data, wrote the initial draft, and edited the manuscript. JMT, CA, KLC, and MD provided supervision in data analysis, methodology, and managed data collection. GKL contributed additional data. BRA facilitated data collection in the field. All authors reviewed and edited the manuscript.

Competing interests

One of the authors is a member of the Editorial Board of *Earth Surface Dynamics*.

Acknowledgements

We owe special thanks to Bhairab Sitaula for invaluable help during field visits and for managing the suspended sediment sample campaign on site. Furthermore, we particularly thank our local partners Deepak Thapa, Shiva Hari Basnet, Radha Krishna Shresta, and Hari Bahadur Karki for collecting the suspended sediment samples. We also thank Stefan Liening, Bernhard Zimmermann, Carolin Zorn, Erez Schmerler, Jonas Krus, Amelia Huang, Bijay Puri, Melanie Stammler, Cristina Gherciu, Till Arnold, Will Reis, and Paul Strobel for sediment sample preparation and grain size measurements in the SedLab at the GFZ. We are grateful to Niels Hovius for discussions and comments on the manuscript. Moreover, we are thankful to Josh West and Marin Clark for assistance in collecting landslide samples.

References

Adhikari, L.B., Gautam, U.P., Koirala, B. P., Bhattarai, M., Kandel, T., Gupta, R. M., et al. (2015). The aftershock sequence of the 2015 April 25 Gorkha–Nepal earthquake, Geophysical Journal International, Volume 203, Issue 3, December 2015, Pages 2119-2124, https://doi.org/10.1093/gji/ggv412

Allen, P. A., Armitage, J. J., Whittaker, A. C., Michael, N. A., Roda-Boluda, D., & D'Arcy, M. (2015). Fragmentation Model of the Grain Size Mix of Sediment Supplied to Basins. The Journal of Geology, 123:405–427

Andermann, C., Bonnet, S., & Gloaguen, R. (2011). Evaluation of precipitation data sets along the Himalayan front. Geochemistry, Geophysics, Geosystems, 12(7).

Andermann, C., Crave, A., Gloaguen, R., Davy, P., & Bonnet, S. (2012). Connecting source and transport: Suspended sediments in the Nepal Himalayas. Earth and Planetary Science Letters, 351-352:158–170.

Andermann, C. & Gloaguen, R. (2009). Estimation of erosion in tectonically active orogenies. Example from the Bhotekoshi catchment, Himalaya (Nepal). International Journal of Remote Sensing, 30(12):3075–3096.

Andermann, Christoff; Puhl, David; Zimmermann, Bernhard; Hughes, Genevieve; Sitaula, Ambika Prasad; Adhikari, Basanta R.; Baidya, Krishna Pyari (2024): PRESSurE suspended sediment data time series, Gorkha earthquake, Nepal. GFZ Data Services. https://doi.org/10.5880/GFZ.4.6.2023.001

Armitage, J. J., Duller, R. A., Whittaker, A. C., & Allen, P. A. (2011). Transformation of tectonic and climatic signals from source to sedimentary archive. Nature Geoscience, 4:231–235.

Attal, M., and J. Lave´ (2009), Pebble abrasion during fluvial transport: Experimental results and implications for the evolution of the sediment load along rivers, J. Geophys. Res., 114, F04023, doi:10.1029/2009JF001328.

Attal, M., Mudd, S. M., Hurst, M. D., Weinman, B., Yoo, K., & Naylor, M. (2015). Impact of change in erosion rate and landscape steepness on hillslope and fluvial sediments grain size in the Feather River basin (Sierra Nevada, California). Earth Surface Dynamics, 3:201–222.

Avouac, J.-P., Meng, L., Wei, S., Wang, T., & Ampuero, J.-P. (2015). Lower edge of locked Main Himalayan Thrust unzipped by the 2015 Gorkha earthquake. Nature Geosci 8, 708–711 (2015). https://doi.org/10.1038/ngeo2518

Begét, J. (1990). Middle Wisconsinan Climate Fluctuations Recorded in Central Alaskan Loess. Géographie physique et Quaternaire, 44(1), 3–13. https://doi.org/10.7202/032793ar

Benda, L. & Dunne, T. (1997). Stochastic forcing of sediment supply to channel networks from landsliding and debris flow. Water Resources Research, 33(12):2865–2880

Bilham, R. (2004). Earthquakes in India and the Himalaya: Tectonics, geodesy and history. Annals of Geophysics, 47(2-3):839–858.

Bollinger, L., Tapponnier, P., Sapkota, S.N. & Klinger, Y. (2016). Slip deficit in central Nepal: omen for a repeat of the 1344 AD earthquake? Earth Planets Space 68, 12 (2016). https://doi.org/10.1186/s40623-016-0389-1

Bookhagen, B., & Burbank, D. W. (2006). Topography, relief, and TRMM-derived rainfall variations along the Himalaya. *Geophysical Research Letters*, *33*(8). https://doi.org/10.1029/2006GL026037

Burrows, K., Marc, O., & Andermann, C. (2023). Retrieval of monsoon landslide timings with Sentinel-1 reveals the effects of earthquakes and extreme rainfall. Geophysical Research Letters, 50, e2023GL104720. https://doi.org/10.1029/2023GL104720

Chen, CM., Hollingsworth, J., Clark, M.K. et al. Erosional cascade during the 2021 Melamchi flood. Nat. Geosci. 18, 32–36 (2025). https://doi.org/10.1038/s41561-024-01596-x

Cook, K. L., Andermann, C., Gimbert, F., Adhikari, B. R., & Hovius, N. (2018). Glacial lake outburst floods as drivers of fluvial erosion in the Himalaya. Science, 362:53–57.

Dadson, S. J., Hovius, N., Chen, H., Dade, W. B., Lin, J. C., Hsu, M. L., et al. (2004). Earthquake-triggered increase in sediment delivery from an active mountain belt. Geology, 32(8):733–736.

Dahlquist, M. P., & West, A. J. (2019). Initiation and runout of post-seismic debris flows: Insights from the 2015 Gorkha Earthquake. Geophysical Research Letters, 46, 9658–9668. https://doi.org/10.1029/2019GL083548

Department of Hydrology and Meteorology Nepal (n. d.). Monsoon Onset and Withdrawal date. Ministry of Energy, Water Resources and Irrigation Department of Hydrology and Meteorology Babarmahal, Kathmandu, Nepal. https://nepalindata.com/media/resources/items/13/bMONSOON_ONSET_AND_WITHDRAWAL_DATE.pdf last access: 18.11.2022.

Department of Hydrology and Meteorology (2025). Retrieved May 25, 2026, from https://dhm.gov.np/uploads/dhm/climateService/Monsoon_seasonal_2025.pdf. Last access: May 25, 2026.

Dietze, E. & Dietze, M. (2019a). Grain-size distribution unmixing using the R package EMMAgeo. E&G Quaternary Science Journal, 68(1):29–46.

Dietze, E and Dietze, M. (2019b). EMMAgeo. GFZ Data Services. R package version 0.9.8. http://doi.org/10.5880/GFZ.4.6.2019.002.

Dietze, E., Hartmann, K., Diekmann, B., IJmker, J., Lehmkuhl, F., Opitz, S., et al. (2012). An end-member algorithm for deciphering modern detrital processes from lake sediments of Lake Donggi Cona, NE Tibetan Plateau, China. Sedimentary Geology, 243-244:169–180.

Dietze, E., Maussion, F., Ahlborn, M., Diekmann, B., Hartmann, K., Henkel, K., et al. (2014). Sediment transport processes across the Tibetan Plateau inferred from robust grain-size end members in lake sediments. Climate of the Past, 10(1):91–106.

Dingle, E. H., Attal, M., & Sinclair, H. D. (2017). Abrasion-set limits on Himalayan gravel flux. Nature, 544(7651):471–474.

Dietze, M., Schulte, P., & Dietze, E. (2022). Application of end-member modelling to grain-size data: Constraints and limitations. *Sedimentology*, *69*(2), 845–863. https://doi.org/10.1111/sed.12929

https://doi.org/10.5194/egusphere-2026-4202
Preprint. Discussion started: 14 August 2026

Dingle, E. H., Sinclair, H., Venditti, J., Attal, M., Kinnaird, T., Creed, M., Quick, L., Nittrouer, J. and D. Gautam (2020) "Sediment dynamics across gravel-sand transitions: Implications for river stability and floodplain recycling". Geology, Vol. 48, DOI: https://doi.org/10.1130/G46909.1

Elliott, J.R., et al.., 2016. Himalayan megathrust geometry and relation to topography revealed by the Gorkha earthquake. Nature Geoscience, 9(2), pp.174-180.

Folk, R.L. & Ward, W.C. (1957) A Study in the Significance of Grain-Size Parameters. Journal of Sedimentary Petrology, 27, 3-26. https://doi.org/10.1306/74D70646-2B21-11D7-8648000102C1865D

Flemming, B.W., (2017) The influence of grain-size analysis methods and sediment mixing on curve shape and textural parameters: Implications for sediment trend analysis. Sed. Geol. 202, 425–435

Gabet, E. J., Burbank, D. W., Pratt-Sitaula, B., Putkonen, J., & Bookhagen, B. (2008). Modern erosion rates in the High Himalayas of Nepal. Earth and Planetary Science Letters, 267(3-4):482–494.

Ghazoui, Z., Bertrand, S., Vanneste, K., Yokoyama, Y., Nomade, J., Gajurel, A. P., & van der Beek, P. A. (2019). Potentially large post-1505 AD earthquakes in western Nepal revealed by a lake sediment record. Nat Commun 10, 2258. https://doi.org/10.1038/s41467-019-10093-4

Gnyawali, K. R. & Adhikari, B. R. (2017). Spatial Relations of Earthquake Induced Landslides Triggered by 2015 Gorkha Earthquake Mw = 7.8. In: Mikoš, M., Casagli, N., Yin, Y., Sassa, K. (eds) Advancing Culture of Living with Landslides. WLF 2017. Springer, Cham. https://doi.org/10.1007/978-3-319-53485-5_10

Haddadchi, A., Ryder, D. S., Evrard, O. & Olley, J. (2013). Sediment fingerprinting in fluvial systems: review of tracers, sediment sources and mixing models. International Journal of Sediment Research. Volume 28, Issue 4, https://doi.org/10.1016/S1001-6279(14)60013-5.

Hannah, D. M., Kansakar, S. R., Gerrard, A. J., & Rees, G. (2005). Flow regimes of Himalayan rivers of Nepal: Nature and spatial patterns. Journal of Hydrology, 308(1- 4):18–32.

Hovius, N., Meunier, P., Lin, C. W., Chen, H., Chen, Y. G., Dadson, S., et al. (2011). Prolonged seismically induced erosion and the mass balance of a large earthquake. Earth and Planetary Science Letters, 304(3-4):347–355.

Hovius, N., Stark, C. P., & Allen, P. A. (1997). Sediment flux from a mountain belt derived by landslide mapping. Geology, 25(3):231–234.

Hovius, N., Stark, C. P., Hao-Tsu, C., & Jiun-Chuan, L. (2000). Supply and Removal of Sediment in a Landslide Dominated Mountain Belt: Central Range, Taiwan. The Journal of Geology, 108:73–89.

Illien, L., Sens-Schönfelder, C., Andermann, C., Marc, O., Cook, K.L., Adhikari, L. B., & Hovius, N. (2022). Seismic velocity recovery in the subsurface: Transient damage and groundwater drainage following the 2015 Gorkha earthquake, Nepal. Journal of Geophysical Research: Solid Earth, 127, e2021JB023402. https://doi. org/10.1029/2021JB023402

Illien, L., Turowski, J.M., Sens-Schönfelder, C. et al. Predictable recovery rates in near-surface materials after earthquake damage. Nat Commun 16, 1790 (2025). https://doi.org/10.1038/s41467-025-57151-8

https://doi.org/10.5194/egusphere-2026-4202
Preprint. Discussion started: 14 August 2026

Kargel, J. S., Leonhard, G. J., Shugar, D. H., Haritashya, U. K., Bevington, A., Fielding, E. J., et al. (2016). Geomorphic and geologic controls of geohazards induced by Nepal's 2015 Gorkha earthquake. Science, 351(6269). https://doi.org/10.1126/science.aac8353

Keefer, D. K. (1984). Landslides caused by earthquakes. Geological Society of America Bulletin, 95:406–421.

Keefer, D. K. (1994). The importance of earthquake-induced landslides to long-term slope erosion and slope-failure hazards in seismically active regions. Geomorphology, 10:265–284.

Kellerhals, R., & Bray, D.I. (1971). Sampling Procedures for Coarse Fluvial Sediments. Journal of Hydraulic Engineering, 97, 1165-1180.

Kobayashi, T., Morishita, Y. & Yarai, H. Detailed crustal deformation and fault rupture of the 2015 Gorkha earthquake, Nepal, revealed from ScanSAR-based interferograms of ALOS-2. Earth Planets Space 67, 201 (2015). https://doi.org/10.1186/s40623-015-0359-z

Knight, A. C. G., Stevenson E. I., Bridgestock, L., Baronas. J. J., Knapp, W. J., Adhikari, B. R., Andermann, C., Tipper, E. T. (2024) The impact of adsorption–desorption reactions on the chemistry of Himalayan rivers and the quantification of silicate weathering rates. Earth and Planetary Science Letters. Volume 641. https://doi.org/10.1016/j.epsl.2024.118814.

Koi, T., Hotta, N., Ishigaki, I., Matuzaki, N., Uchiyama, Y., & Suzuki, M. (2008). Prolonged impact of earthquake-induced landslides on sediment yield in a mountain watershed: The Tanzawa region, Japan. Geomorphology, 101:692–702.

Koketsu, K., Miyake, H., Guo, Y., Kobayashi, H., Masuda, T., Davuluri, S., et al. Widespread ground motion distribution caused by rupture directivity during the 2015 Gorkha, Nepal earthquake. Sci Rep 6, 28536 (2016). https://doi.org/10.1038/srep28536

Kincey, M. E., Rosser, N. J., Robinson, T. R., Densmore, A. L., Shrestha, R., Pujara, D. S., et al. (2021). Evolution of coseismic and post-seismic landsliding after the 2015 Mw 7.8 Gorkha earthquake, Nepal. Journal of Geophysical Research: Earth Surface, 126, e2020JF005803. https://doi.org/10.1029/2020JF005803

Kumar, S., S. G. Wesnousky, T. K. Rockwell, R. W. Briggs, V. C. Thakur, and R. Jayangondaperumal (2006), Paleoseismic evidence of great surface rupture earthquakes along the Indian Himalaya, J. Geophys. Res.,111, B03304,doi:10.1029/2004JB003309.

Larsen, I. & Montgomery, D. (2012). Landslide erosion coupled to tectonics and river incision. Nature Geosci 5, 468–473 (2012). https://doi.org/10.1038/ngeo1479

Li, G., West, A. J., Densmore, A. L., Hammond, D. E., Jin, Z., Zhang, F., et al. (2016). Connectivity of earthquake-triggered landslides with the fluvial network: Implications for landslide sediment transport after the 2008 Wenchuan earthquake. Journal of Geophysical Research: Earth Surface, 121:703–724.

Li, G., West, A. J., Densmore, A. L., Jin, Z., Parker, R. N., & Hilton, R. G. (2014). Seismic mountain building: Landslides associated with the 2008 Wenchuan earthquake in the context of a generalized model for earthquake volume balance. Geochemistry, Geophysics, Geosystems, 15(4):833–844.

Li, G.K., West, A.J., Jin, Z. et al. (2025) Large riverbed sediment flux sustained for a decade after an earthquake. Nature 644, 398–403. https://doi.org/10.1038/s41586-025-09354-8

Li, G., West, A. J., & Qiu, H. (2019). Competing effects of mountain uplift and landslide erosion over earthquake cycles. Journal of Geophysical Research: Solid Earth,124, 5101–5133. https://doi.org/10.1029/2018JB016986

Lin, G.-W., Chen, H., Hovius, N., Horng, M. J., Dadson, S., Meunier, P., & Lines, M. (2008). Effects of earthquake and cyclone sequencing on landsliding and fluvial sediment transfer in a mountain catchment. Earth Surface Processes and Landforms, 33:1354–1373

Lukens, C. E., Riebe, C. S., Sklar, L. S., & Shuster, D. L. (2023). Sand, gravel, cobbles, and boulders: Detrital thermochronology shows that one size does not tell all. Journal of Geophysical Research: Earth Surface, 128, e2023JF007192. https://doi. org/10.1029/2023JF007192

Lupker, M., Blard, P.-H., Lavé, J., France-Lanord, C., Leanni, L., Puchol, N., et al. (2012). 10Be-derived Himalayan denudation rates and sediment budgets in the Ganga basin. Earth and Planetary Science Letters. Volumes 333–334. Pages 146-156. https://doi.org/10.1016/j.epsl.2012.04.020.

Nepal, S. (2016) Impacts of climate change on the hydrological regime of the Koshi river basin in the Himalayan region. Journal of Hydro-environment Research. Volume 10. https://doi.org/10.1016/j.jher.2015.12.001.

Märki, L., Lupker, M., France-Lanord, C., Lavé, J., Gallen, S., Gajurel, A. P., Haghipour, N., Leuenberger-West, F., Eglinton, T. (2021) An unshakable carbon budget for the Himalaya, Nature Geoscience, 10.1038/s41561-021-00815-z, 14, 10, (745-750), (2021).

Marc, O., Turowski, J. M., and Meunier, P. (2021): Controls on the grain size distribution of landslides in Taiwan: the influence of drop height, scar depth and bedrock strength, Earth Surf. Dynam., 9, 995–1011, https://doi.org/10.5194/esurf-9-995-2021.

Marc, O., Behling, R., Andermann, C., Turowski, J. M., Illien, L., Roessner, S., & Hovius, N. (2019). Long-term erosion of the Nepal Himalayas by bedrock landsliding: the role of monsoons, earthquakes and giant landslides. Earth Surface Dynamics, 7(1):107–128.

Marc, O., Hovius, N., & Meunier, P. (2016). The mass balance of earthquakes and earthquake sequences. Geophysical Research Letters, 43:3708–3716.

Marc, O., Hovius, N., Meunier, P., Uchida, T., & Hayashi, S. (2015). Transient changes of landslide rates after earthquakes. Geology, 43(10):883–886.

Martha, T. R., Roy, P., Mazumdar, R., Govindharaj, K. B. & Kumar, K. V. (2017). Spatial characteristics of landslides triggered by the 2015 Mw 7.8 (Gorkha) and Mw 7.3 (Dolakha) earthquakes in Nepal. Landslides 14, 697–704 (2017). https://doi.org/10.1007/s10346-016-0763-x

Martin, Y., Rood, K., Schwab, J. W., & Church, M. (2002). Sediment transfer by shallow landsliding in the Queen Charlotte Islands, British Columbia. Canadian Journal of Earth Sciences, 39:189–205.

Meunier, P., Hovius, N., & Haines, A. J. (2007). Regional patterns of earthquaketriggered landslides and their relation to ground motion. Geophysical Research Letters, 34:1–5.

Meunier, P., Hovius, N., & Haines, J. A. (2008). Topographic site effects and the location of earthquake induced landslides. Earth and Planetary Science Letters, 275(3- 4):221–232.

Morin, G. P., Lave, J., France-Lanord, C., Rigaudier, T., Gajurel, A. P., & Sinha, R. (2018). Annual Sediment Transport Dynamics in the Narayani Basin, Central Nepal: Assessing the Impacts of Erosion Processes in the Annual Sediment Budget. Journal of Geophysical Research: Earth Surface, 123(10):2341–2376.

Parker, R. N., Densmore, A. L., Rosser, N. J., De Michele, M., Li, Y., Huang, R., et al. (2011). Mass wasting triggered by the 2008 Wenchuan earthquake is greater than orogenic growth. Nature Geoscience, 449-452.

Parker, R. N., Hancox, G. T., Petley, D. N., Massey, C. I., Densmore, A. L., & Rosser, N. (2015). Spatial distributions of earthquake-induced landslides and hillslope preconditioning in the northwest South Island, New Zealand, Earth Surf. Dynam., 3, 501–525, https://doi.org/10.5194/esurf-3-501-2015, 2015.

Pearce, A. J. & Watson, A. J. (1986). Effects of earthquake-induced landslides on sediment budget and transport over a 50-yr period. Geology, 14:52–55.

Pokhrel, P., Attal, M., Sinclair, H. D., Mudd, S. M., and Naylor, M.: Downstream rounding rate of pebbles in the Himalaya, Earth Surf. Dynam., 12, 515–536, https://doi.org/10.5194/esurf-12-515-2024, 2024.

Riebe, C. S., Sklar, L. S., Lukens, C. E., & Shuster, D. L. (2015). Climate and topography control the size and flux of sediment produced on steep mountain slopes. Proceedings of the National Academy of Sciences, 112(51):15574–15579.

Roback, K., Clark, M. K., West, A. J., Zekkos, D., Li, G., Gallen, S. F., et al. (2018). The size, distribution, and mobility of landslides caused by the 2015 M w 7.8 Gorkha earthquake, Nepal. Geomorphology, 301:121–138.

Roda-Boluda, D. C., D'Arcy, M., McDonald, J., & Whittaker, A. C. (2018). Lithological controls on hillslope sediment supply: insights from landslide activity and grain size distributions. Earth Surface Processes and Landforms, 43:956–977.

Rosser, N., Kincey, M. E., Oven, K., Densmore, A., Robinson, T., Pujara, D. S. et al. (2021). Changing significance of landslide Hazard and risk after the 2015 Mw 7.8 Gorkha, Nepal Earthquake, Progress in Disaster Science, Volume 10, 2021, 100159, ISSN 2590-0617, https://doi.org/10.1016/j.pdisas.2021.100159.

Saidi, I. S., Jacques, S. L., and Tittel, F. K. (1995) "Mie and Rayleigh modeling of visible-light scattering in neonatal skin," Appl. Opt. 34, 7410-7418

Sassolas-Serrayet, T., Cattin, R., & Ferry, M. (2018). The shape of watersheds. *Nature Communications*, *9*(1), 3791. https://doi.org/10.1038/s41467-018-06210-4

Schwanghart, W., Bernhardt, A., Stolle, A., Hoelzmann, P., Adhikari, B. R., Andermann, C., et al. (2016). Repeated catastrophic valley infill following medieval earthquakes in the Nepal Himalaya. Science, 351 (2016), pp. 147-150. https://doi.org/10.1126/science.aac9865

https://doi.org/10.5194/egusphere-2026-4202
Preprint. Discussion started: 14 August 2026

Sinha, R., Gupta, A., Mishra, K., Tripathi, S., Nepal, S., Wahid, S. M., Swarnkar, S. (2019) Basin-scale hydrology and sediment dynamics of the Kosi river in the Himalayan foreland. Journal of Hydrology. Volume 570. https://doi.org/10.1016/j.jhydrol.2018.12.051.

Sklar, L. S., Riebe, C. S., Genetti, J., Leclere, S. & Lukens, C. E. (2020). Downvalley fining of hillslope sediment in an alpine catchment: implications for downstream fining of sediment flux in mountain rivers. Earth Surface Processes and Landforms. Vol

Sklar, L. S., Riebe, C. S., Marshall, J. A., Genetti, J., Leclere, S., Lukens, C. L., & Merces, V. (2017). The problem of predicting the size distribution of sediment supplied by hillslopes to rivers. Geomorphology, 277:31–49.

Struck, M., Andermann, C., Hovius, N., Korup, O., Turowski, J. M., Bista, R., et al. (2015). Monsoonal hillslope processes determine grain sizespecific suspended sediment fluxes in a trans-Himalayan river. Geophysical Research Letters, 42:2302–2308.

Talchabhadel, R., Karki, R., Thapa, B. R., Maharjan, M. & Parajuli, B. (2018). Spatio-temporal variability of extreme precipitation in Nepal. Int. J. Climatol., 38 (2018), pp. 4296. https://doi.org/10.1002/joc.5669

Tanyaş, H., van Westen, C. J., Allstadt, K. E., Nowicki Jessee, M. A, Görüm, T., Jibson, R. W., et al. (2017). Presentation and analysis of a world-wide database of earthquake-induced landslide inventories. Journal of Geophysical Research: Earth Surface,122,1991–2015. https://doi.org/10.1002/2017JF004236

Tian, Y., Owen, L. A., Xu, C., Shen, L., Zhou, Q. & Figueiredo, P. M. (2020). Geomorphometry and Statistical Analyses of Landslides Triggered by the 2015 Mw 7.8 Gorkha Earthquake and the Mw 7.3 Aftershock, Nepal. Front. Earth Sci. 8:572449. doi: 10.3389/feart.2020.572449

Tiwari, B., Ajmera, B., & Dhital, S. (2017). Characteristics of moderate-to large-scale landslides triggered by the Mw 7.8 2015 Gorkha earthquake and its aftershocks, Landslides, doi: 10.1007/s10346-016-0789-0

Tofelde, S., Duesing, W., Schildgen, T., Wickert, A. D., Wittmann, H., Alonso, R. N. & Strecker, M. (2018): Effects of deep-seated versus shallow hillslope processes on cosmogenic 10Be concentrations in fluvial sand and gravel. Earth Surface Processes and Landforms, 43, 15, pp. 3086— 3098. DOI: http://doi.org/10.1002/esp.4471

Tofelde S, Bernhardt A, Guerit L, and Romans BW (2021) Times Associated with Source-to-Sink Propagation of Environmental Signals During Landscape Transience. Front. Earth Sci. 9:628315. doi 10.3389/feart.2021.628315

Vandenberghe, J., An, Z.S., Nugteren, G., Lu, H. Y. & Van Huissteden, K., 1997. New absolute time scale for the Quaternary climate in the Chinese loess region by grain-size analysis. Geology 25, 35-38.

Vandenberghe, J.F., Mücher, H.J., Roebroeks, W. & Gemke, D., 1985. Lithostratigraphy and palaeoenvironment of the Pleistocene deposits at Maastricht-Belvedere, southern Limburg, The Netherlands. Mededelingen Rijksgeologische Dienst 39 (1), 7–29

V. A. Vanoni, V. A. (1975) "Sedimentation Engineering," American Society of Civil Engineers, New York, 1975.

Valagussa, A., Frattini, P., Valbuzzi, E. & Crosta, G. B. (2021). Role of landslides on the volume balance of the Nepal 2015 earthquake sequence. Sci Rep 11, 3434. https://doi.org/10.1038/s41598-021-83037-y

Wang, J., Jin, Z., Hilton, R. G., Zhang, F., Densmore, A. L., Li, G., & Joshua West, A. (2015). Controls on fluvial evacuation of sediment from earthquake-triggered landslides. Geology, 43(2):115–118.

Wang, J., Jin, Z., Hilton, R. G., Zhang, F., Li, G., Densmore, A. L., Gröcke, D. R., et al. (2016). Earthquake-triggered increase in biospheric carbon export from a mountain belt. Geology, 44(6):471–474.

Weltje, G. J. & Prins, M. A (2007): Genetically meaningful decomposition of grain-size distributions, Sediment. Geol., 202, 409–424.

Whittaker, A. C., Attal, M., & Allen, P. A. (2010). Characterising the origin, nature and fate of sediment exported from catchments perturbed by active tectonics. Basin Research, 22:809–828.

Williams, J. G., Rosser N. J., Kincey, M. E., Benjamin, J., Oven, K. J., Densmore, A. L., et al. (2018). Satellite-based emergency mapping using optical imagery: experience and reflections from the 2015 Nepal earthquakes. Nat Hazards Earth Syst Sci, 18, pp. 185-205

Xu, C., Xu, X., Tian, Y., Shen, L., Yao, Q., Huang, X., et al. (2016). Two comparable earthquakes produced greatly different coseismic landslides: The 2015 Gorkha, Nepal and 2008 Wenchuan, China events. J. Earth Sci. 27, 1008–1015 (2016). https://doi.org/10.1007/s12583-016-0684-6

Yang, W., Qi, W., Wang, M., Zhang, J. & Zhang, Y., (2017). Spatial and temporal analyses of post-seismic landslide changes near the epicentre of the Wenchuan earthquake.
Geomorphology 276, 8–15. https://doi.org/10.1016/j.geomorph.2016.10.010.

Yanites, B.J., Tucker, G.E., Mueller, K.J. & Chen, Y.-G., 2010. How rivers react to large earthquakes: evidence from Central Taiwan. Geology 38, 639–642. https://doi.org/10.1130/G30883.1.

Yanites, B. J. et al. Cascading land surface hazards as a nexus in the Earth system. Science 388, eadp9559 (2025). DOI:10.1126/science.adp9559

Zeichner, S. S., Nghiem, J., Lamb, M. P., Takashima, N., de Leeuw, J., Ganti, V., & Fischer, W. W. (2021). Early plant organics increased global terrestrial mud deposition through enhanced flocculation. Science, 371(6528), 526– 529. https://doi.org/10.1126/science.abd0379

Zekkos, D., Clark, M., Whitworth, M., Greenwood, W., West, A. J., Roback, K., et al. (2017). Observations of landslides caused by the April 2015 Gorkha, Nepal, Earthquake Based on land, UAV, And satellite reconnaissance. Earthquake Spectra, 33 (Special issue 1):95–114.

Zhang, H., van der Lee, S. & Ge, Z., (2016). Multiarray rupture imaging of the devastating 2015 Gorkha, Nepal, earthquake sequence, Geophys. Res. Lett.,43, 584–591, doi:10.1002/2015GL066657.

Zhang, F., Zhangdong, J., West, A. J., Zhisheng, A., Hilton, R. G., Wang, J., et al. (2019). Monsoonal control on a delayed response of sedimentation to the 2008 Wenchuan earthquake. Science Advances. Vol. 5. Issue 6. doi:10.1126/sciadv. aav7110